Use of 4,4'-diamino diphenyl methane to derive a novel series of diamines and their ensuing metallomacrocyclic complexes: Synthesis, characterization, DFT and *in vitro* cytotoxic study against Hep G2 cancer cell line

Abstract

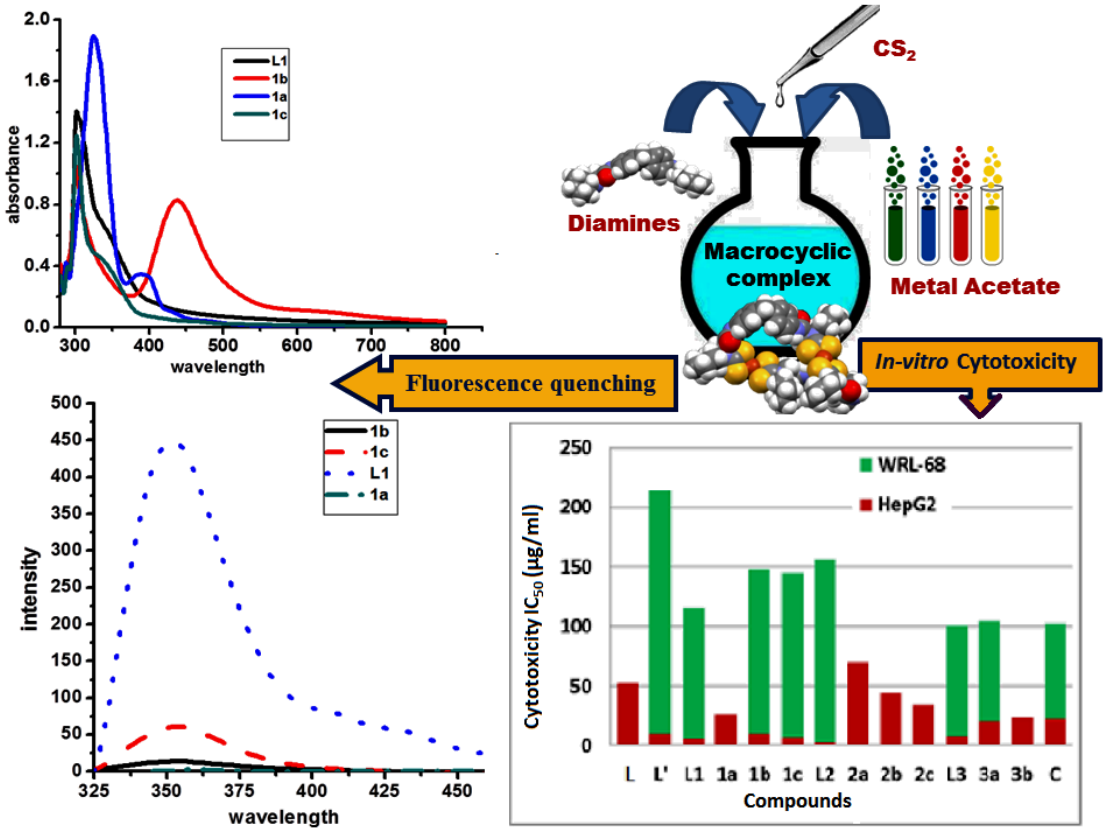

Three 2° diamine precursors 4,4'-bis(2-(alkylamino)acetamido)diphenylmethane (L^1–L^3) have been prepared and characterized in well prior to use. A self-assembly process involving these amino precursors, CS_2 and Ni^{II}, Cu^{II} or Zn^{II} affords access to a new series of binuclear metallomacrocyclic complexes [M_2-μ^2-bis-{(κ^2S,S-$S_2CN(R)CH_2CONHC_6H_4)_2CH_2$}] {R = *Cy*, M = Ni^{II}1a, Cu^{II}1b, Zn^{II}1c; R = ^{i}Pr, M = Ni^{II}2a, Cu^{II}2b, Zn^{II}2c; R = ^{n}Bu, M = Ni^{II}3a, Cu^{II}3b, Zn^{II}3c}. All the compounds were

suitably characterized by spectroscopic (^{1}H, ^{13}C, DEPT 135, ^{1}H DOSY NMR, ESI MS, UV-visible absorption, IR) and thermogravimeteric methods and experimental results were further supported by a DFT level calculation. Evidently **L^1-L^3** fluoresces well in the range of 302–430, however, their fluorescence property is thoroughly quenched by Ni^{II}, Cu^{II} and even by Zn^{II} ions in their corresponding metal complexes. All the compounds were screened for their possible *in vitro* cytotoxic activity against malignant tumors Hep G2 (hepatoma) cell lines by the MTT assay. The results showed better activity of many compounds (**L'**, **L^1-L^3**, **1b**, **1c**, **3a**) than clinically used drug cisplatin and these compounds evidently showed specificity for cancer cells over normal liver cells under similar experimental condition. Exceptionally, ligand precursor L^2 holding *N*-^{i}Pr substituents shows nearly 7 fold better cytotoxic activity against Hep G2 (2.95 ± 0.03 µg/ml) cell lines, compared to the reference drug Cisplatin. The shrinking of cells can be clearly visualized by acridine orange/ethidium bromide (AO/EB) staining indicating the induction of apoptosis as part of the mechanism of action of these compounds. All the complexes are electro active mainly with respect to the coordinated ligands and the metal centers are present in silent mode, except Cu^{II} complexes.

3.1 Introduction

Over few decades, considerable attention has been paid to develop effective chemo-therapeutic agents bearing macrocyclic motif that can either be a suitable drug[1] or effective in drug-delivery.[2] The encapsulation protects the drug molecules from intracellular degradation and reduce glutathione deactivation drastically.[3a] Further report suggests that encapsulated complexes showed tolerated dose doubled in mice, compared with non-macrocycle treated drugs.[3b] Structural pre-organization with sufficient flexibility for better binding along with high degree of potency and selectivity have been shown by such motifs during interaction with the target molecules in biological systems.[4]

However, the majority of the synthesized compounds is inadequate for the use as chemotherapeutic agents because of the following reasons: (i) lack of suitable chemical structure for the appropriate structural modification; (ii) limited cytotoxicity and high

toxicity; (iii) difficulties in transportation and addressing the molecule to the targets; (iv) protection of the pharmacophore against untimely exchanges with biomolecules. Chemists undertake this ever challenging task to develop an efficient synthetic methodology to bring varied pharmacophores viz. Transition metal ions, sulfur atoms and other active groups within a single molecular platform to overcome these issues (vide supra). The ability of transition metal ions to show variable coordination numbers, geometries, redox states, thermodynamic-kinetic characteristics can offer additional opportunities for development of new therapeutic agents which are indeed not accessible to organic compounds. The sulfur atoms of 1,1-dithio ligands play a crucial role in transporting and addressing the molecule to the targets as well as in the protection of the pharmacophore against untimely exchanges with biomolecules.[5,6] Literature supports good DNA/protein binding/cleaving and catalytic activity of sulfur-rich compounds with glutathione.[7]

Beer's *et al*[8,30] have successfully used coordination driven self-assembly of 1,1-dithiocarbamate ligands with transition metal ions to derive a number of metallomacrocyclic structures that have been studied widely in the supramolecular chemistry. Such system has projected a series of different applications such as selective molecular and ion recognition, separation, storage, transport and catalysis.[9a] A variety of guest substrates have been encapsulated and stabilized by metallomacrocyclic structures as well as chemical reactions have been catalyzed, within these "micro reactor" cores.[9b] My research group has successfully utilized 4,4'-diaminodiphenylether and 4,4'-diaminodiphenylsulfone to derive a number of bisimines, diamines, bimetallic metallomacrocyclic structures and have systematically investigated these derivatives from medicinal perspectives.[10]

A careful literature search reveals the cytotoxic effects of 4,4'-diaminodiphenylmethane on hepatocarcinogenesis in male F344 rats. The report clearly suggests the reduction in liver tumor incidence post administration of 4,4'-diaminodiphenylmethane.[11] An intraperitoneal injection of 4,4'-diaminodiphenylmethane into mice reaches its peak blood concentration in 10 minutes with the elimination half-life of 3.2 hours.[12] Tanaka et al. reported that the oral administration of 4,4'-diaminodiphenylmethane to mice in doses of 50 mg/kg, the N-

acetyl derivative/ N,N'-diacetyl derivative were eliminated through urine within 72 hours.[13] A structural combination of diaminodiphenylmethane along with hydrophobic substituents on the nitrogen atoms in GN8 derivatives is responsible for the antiprion activity in TSE-infected cells.[14] These findings and suitability of 4,4'-diaminodiphenylmethane for the appropriate derivatization have encouraged us to select 4,4'-diaminodiphenylmethane as a lead compound (L) for further study. Pointing towards better hepatocytotoxic potential of L, it was pertinent to derivatise L into a number of organic diamines viz. 4,4'-bis(2-(cyclohexylamino)acetamido)diphenylmethane (L^1), 4,4'-bis(2-(isopropylamino)acetamido) diphenylmethane (L^2), 4,4'-bis(2-(n-butylamino)acetamido)diphenyl methane (L^3) and their ensuing metallomacrocyclic dithiocarbamate complexes [M_2-μ^2-bis-{(κ^2S,S-$S_2CN(R)CH_2CONHC_6H_4)_2CH_2$}]. Hep G2 cell line was selected for the evaluation because liver is a major site of synthesis and metabolism of major biomolecules like proteins and carbohydrates. It shows the ability to metabolize, detoxify and inactivate exogenous compounds such as drugs, other exogenous and also endogenous compounds like steroids.

This paper presents the synthesis, spectroscopic characterization, thermogravimetric analysis, fluorescence, electrochemical study, density functional theory calculations and biological reactivity of a number of derivatives of 4,4'-diaminodiphenylmethane viz. L', L^1-L^3 and [M_2-μ^2-bis-{(κ^2S,S-$S_2CN(R)CH_2CONHC_6H_4)_2CH_2$}] {R = *Cy*, M = Ni^{II}1a, Cu^{II}1b, Zn^{II}1c; R = ^{i}Pr, M = Ni^{II}2a, Cu^{II}2b, Zn^{II}2c; R = ^{n}Bu, M = Ni^{II}3a, Cu^{II}3b, Zn^{II}3c}. The worth of the present series of compounds would be supplemented by their ease of synthesis, their specificity for cancer cells over normal liver cells and the fluorescence quenching ability of transition metal ions, especially Zn^{II} ions in their corresponding metallomacrocyclic dithiocarbamate complexes.

3.2 Experimental Section

3.2.1. Materials and Instrumentations

Metal acetates were purchased from Merck, 4, 4'-Diaminodiphenyl methane was purchased from National Chemicals and all solvents such as chloroacetylchloride, chloroform, acetonitrile, absolute alcohol, n-hexane were purchased from Chemlab. All other solvents and reagents were of AR grade and have been used without further

purification.The lead precursor 4,4'-bis(2-chloroacetamido)diphenylmethane (**L')** was synthesized from 4,4'-diaminodiphenyl methane by reacting chloroacetyl chloride under mild basic condition following a modified literature procedure. Reactions and manipulations were performed under an inert atmosphere. Melting points were recorded in open capillaries and these are uncorrected. Thin layer chromatography (TLC) was performed on Merck 60 F254 aluminium coated plates to monitor the progress of reaction. ESI MS were obtained on AB SCIEX 3200 Q TRAP LCMS instrument. Infrared (KBr pellets) spectra were recorded in the 4000-400 cm^{-1} range using a Perkin-Elmer FT-IR spectrometer. ^{1}H, ^{13}C, DEPT-135and DOSY NMR spectra were obtained on a Bruker AV-III 400 MHz spectrometer in DMSO-d^6 solvent and chemical shifts are reported in parts per million (ppm). Uv-visible absorption spectra were recorded on a Perkin Elmer Lambda 35 UV-visible spectrophotometer. Fluorescence spectra were recorded on JASCO make spectrofluorometer model FP-6300. Thermogravimetric analysis was carried out on SII TG/DTA 6300 under flowing N_2 with a heating rate of 10 °C min^{-1}. Electrochemical measurements were performed on a CH Instruments 600C potentiostat, using a Pt disk as the working electrode, Ag/AgCl as the reference electrode and a Pt wire as the counter electrode. Voltammograms were recorded by using anhydrous solutions of the ligand precursors and metallomacrocyclic dithiocarbamate complexes in DMF (10^{-3}M) containing tetra-n-butylammoniumhexafluoro phosphate (5×10^{-3}M) as supporting electrolyte.

3.2.2. General synthetic procedure for diamineprecursors 4,4' bis(alkylamino)acetamido)biphenyl methane L^1-L^3

Preparation of 4,4'-bis(2-chloroacetamido)diphenyl methane (L')

Solid $NaHCO_3$ (3 eq.) was added to a clear solution of 4,4'-methylenedianiline (1.0 g, 5.04 mmol) in dichloromethane and the reaction mixure was stirred for 30 minutes. To this solotion, 2-chloroacetyl chloride was added carefully dropwise by using dropping funnel at 0 ˚C over a period of 40 minutes and then allowed to stir at room temperature for 2-3 hours. The progress of reaction was monitored by TLCs. The residue was filtered over glass sintered crucible, washed with 3 × 5 mL of 5% of $NaHCO_3$, 3 × 5 mL of

distilled water followed by hexane. Finally the residue was dried under high vaccum to yield the white coloured 4,4'-bis(2-chloroacetamido)diphenyl methane (L') which was taken for the analysis.

4,4'-bis(2-chloroacetamido)diphenyl methane (L'): MW: 351.23, Yield: 1.505 g, 85%. M.p. 200°C dec. ^{1}HNMR (400 (DMSO-d6, 400 MHz) δ, ppm: 10.57 (s, 4H, NH); 7.54 (d, 4H, Ph); 7.14 (d, 4H, Ph); 4.27 (s, 2H, COC*H*$_2$Cl); 3.84 (s, 2H, Ph-C*H*$_2$-Ph). ^{13}C NMR (400MHz, DMSO-d6) δ ppm: 164.94 (-C=O); 137.23, 137.04, 129.39, 119.92 (C-Ph); 43.99 (*C*H$_2$Cl), 40.39 (Ph-*C*H$_2$-Ph). DEPT-135 (400MHz, DMSO-d6) δ ppm: 129.39, 119.92 (-CH, Ph) ; 43.99 (-CH Cy); 40.39 (Ph-*C*H$_2$-Ph).

An excess amount of cyclohexyl amine (892.2 mg, 9 mmol), isopropylamine (531.9 mg, 9 mmol) or n-butylamine (658.2 mg, 9 mmol), was added to a ethanolic solution of 4,4'-bis(2-chloroacetamido) diphenylmethane (702.4 mg, 2 mmol). The reaction mixture was refluxed in the presence of catalytic amount of Et$_3$Nfor 8 hours and the progress of reaction was examined by TLC. The reaction mixture was cooled to room temperature and further poured on ice, precipitates obtained was filtered and washed with cold water, followed by n-hexane and diethyl ether to produce diamines**L^1-L^3** in good yields. These samples were stored under a N_2 atmosphere and further taken for analysis.

4,4'-bis(2-(cyclohexylamino)acetamido)diphenylmethane (L^1): MW: 476, Yield: 781.5 mg, 82%. m.p. 134 °C. ESI-MS: 474.1 (M-2H). FTIR (KBr disc, cm^{-1}): 3333.35w, 3256.57w, 3039.19w, 2926.20vs, 2851.89m, 1693.94w, 1666.76vs, 1606.47m, 1526.83vs, 1447.96w, 1410.51s, 1373.50w, 1309.66m, 1253.30w, 1131.77m, 1018.38w, 962.49w, 923.13w, 891.53w, 816.24w, 778.94w, 508.83m. ^{1}H NMR (400 MHz, DMSO-d$_6$): δ (ppm) 9.76 (s, 2H, CON*H*); 7.52 (d, 4H, *Ph*); 7.12 (d, 4H, *Ph*); 3.82 (s, 4H, NC*H*$_2$CO); 3.25 (m, 2H, C*H* of Cy); 2.34 (s, 2H, Ph-C*H*$_2$); 1.7 (bs, 2H, N*H*); 1.80-1.02 (m, 20H, *Cy*). ^{13}C NMR (400MHz, DMSO-d6) δ ppm: 171.03 (*C*=O); 137.04, 136.79 (*C*-N), 129.34, 119.58 (*Ph*); 56.74 (*C*H of Cy); 50.66 (NCH$_2$CO); 33.35 (Ph-*C*H$_2$); 26.18, 24.83 (*C*H$_2$ of Cy). DEPT-135 (400MHz, DMSO-d6) δ ppm: 129.34, 119.58 (*Ph*); 56.74 (*C*H of Cy); 50.66 (NCH$_2$CO); 33.35, (Ph-*C*H$_2$), 26.18, 24.83 (*C*H$_2$ of Cy).

4,4'-bis(2-(isopropylamino)acetamido)diphenylmethane (L^2): MW: 396, Yield: 673.9 mg, 85%. m.p. 106°C. ES-MS: 527.1 (M+H). FTIR (KBr disc, cm^{-1}): 3470.65m, 3301.06s, 3120.49w, 3042.74m, 2964.87s, 2870.04w, 1689.79sh, 1669.68s, 1609.66vs, 1530.22vs, 1467.60w, 1410.29vs, 1363.54w, 1309.91m, 1259.54m, 1173.12m, 1094.96w, 1018.45w, 963.95m, 919.55w, 865.48m, 817.73m, 767.87m, 692.55w, 569.87w, 506.76w, 442.22w. ^{1}H NMR:(DMSO-d6, 400 MHz) : δ (ppm) 9.76 (s, 4H, CON*H*); 7.50 (d, 4H, *Ph*); 7.12 (d, 4H, *Ph*); 3.82 (s, 4H, NCH_2CO); 3.23 (s, 2H, C*H* of ^{i}*Pr*); 2.70 (m, 2H, Ph-CH_2); 2.68 (s, br, 2H, N*H*), 0.99-0.97 (m, 12H, -CH_3 of ^{i}*Pr*).^{13}C NMR:(400 MHz, DMSO-d6) δ ppm: 170.90 (*C*=O); 137.04, 136.80 (*C*-N), 129.34, 119.63 (*Ph*) ; 50.99 (N*C*H_2CO); 48.70 (*C*H of ^{i}Pr); 23.16 (-CH_3). (DEPT-135, DMSO-d6) δ ppm: 129.34, 119.63 (*Ph*); 50.99 (N*C*H_2CO); 48.70 (*C*H of ^{i}Pr); 23.16 (*C*H_3 of ^{i}Pr).

4,4'-bis(2-(n-butylamino)acetamido)diphenylmethane (L^3): MW: 424, Yield: 645.1 mg, 76%. m.p. 45 °C. ES-MS: 422.28 (M-2H). FTIR (KBr disc, cm^{-1}): 3498w, 3287.85s, 3117.45w, 3048.37w, 2955.59s, 2926.28s, 2860.87s,1692.81vs, 1671.41vs, 1605.60vs, 1531.87vs, 1456.23w, 1433.11w, 1375.67w, 1308.59vs, 1278.74w, 1249m, 1184.30m 1126.70m, 1019.50m, 994.96w, 916.53w, 860.95m, 816.53s, 776.60m, 733.70w, 601.36w, 507.53s, 430.66w. ^{1}HNMR:(DMSO-d6, 400 MHz) : δ (ppm) 9.76 (s, 4H, CON*H*) ; 7.50 (d, 4H, *Ph*); 7.12 (d, 4H, *Ph*); 3.82 (s, 4H, NCH_2CO); 3.23 (s, 4H, NCH_2 of ^{n}*Bu*); 1.42-1.28 (m, 8H, CH_2 of ^{n}*Bu*); 1.40 (broad s, 2H, N*H*); 0.88-0.847 (m, 6H, CH_3 of ^{n}*Bu*).^{13}C NMR:(400MHz, DMSO-d6) δ ppm: 170.51 (*C*=O); 137.09, 136.79 (*C*-N);129.33, 119.65 (*Ph*); 53.16 (N*C*H_2CO); 49.21 (N*C*H_2 of ^{n}*Bu*); 31.98 (Ph-*C*H_2), 20.32 (*C*H_2 of ^{n}*Bu*) 14.36 (*C*H_3 of Butyl). (DEPT-135, DMSO-d6) δ ppm: 129.33, 119.65 (*C*H of Ph); 53.16 (N*C*H_2CO); 49.21 (N*C*H_2 of ^{n}*Bu*); 31.98 (Ph-*C*H_2); 20.32 (*C*H_2 of ^{n}*Bu*); 14.37 (*C*H_3 of ^{n}Bu).

3.2.3 General Synthetic procedure for metallomacrocyclicdithiocarbamate complexes 1a-1c, 2a-2c, 3a-3c

In a vigorously stirring acetonitrile solution of 1 equivalent of diamine precursor L^1 (0.238 g, 0.5mmol), L^2 (0.198 g, 0.5mmol) or L^3 (0.212 g, 0.5mmol), an excess amount of NaOH (~3 equivalent; ~ 0.060 g) and carbon disulfide (~10 equivalent; ~ 0.5 ml) were

added and stirring was allowedtocontinue for 12 h at room temperature. A change in color from colorless to pale yellow was observed through the advancement of the reaction. Subsequent addition of $Ni^{II}(C_2H_3O_2)_2.4H_2O$ (136 mg, 0.55 mmol), $Cu(C_2H_3O_2)_2.H_2O$ (0.111 g, 0.55 mmol) or $Zn^{II}(C_2H_3O_2)_2.2H_2O$ (121 mg, 0.55mmol), dissolved in a minimum amount of distilled water, was carried out and the reaction mixture was allowed to continue for 8 h at room temperature. The progress of reaction was indeed monitored by thin layer chromatography and by a gradual colour change from colourless to dark green (in case of Ni^{II}), from colourless to dark brown (in case of Cu^{II}) and from colourless to yellow (in case of Zn^{II}). The reaction mixture was vacuum dried and the residue was washed several times with distilled water, followed by n-hexane and diethyl ether. The resultant free flowing powder was dried under vacuum to produce the analogusmacrocyclicdithiocarbamte complexes **1a-1c, 2a-2c, 3a-3c.**

[Ni_2-μ^2-bis-{(κ^2*S,S*-$S_2CN(Cy)CH_2CONHC_6H_4)_2CH_2$}] (1a). Dark green MW: 1371, Yield: 568.3 mg, 83%. m.p. 223°C dec.ES-MS: 1372.8 (M+H). FTIR (KBr disc, cm^{-1}): 3314.58w, 3122.53w, 3030.37w, 2932.39vs. 2854.47m, 2658.10w, 2362.04w, 2092.25m, 1760w, 1692.13vs, 1603.03vs, 1516.06vs, 1471.54vs, 1410.56s, 1351.89w, 1306.30s, 1241.52vs, 1166.88vs, 1138.67w, 1057.04w, 1010.90s, 971.58m, 893.99w, 915.01w, 813.93m, 773.45w, 675.32w, 608.85w, 502.64m, 467.36w, 425.46 w. ^{1}H NMR (DMSO-d_6, 400 MHz): δ (ppm) 10.085 (s, 4H, CON*H*); 7.40-7.09(m, 16H, *Ph*); 4.29 (s, 8H, NCH_2CO); 3.72 (C*H* of Cy); 2.46 (merged with DMSO-d_6, Ph-CH_2); 1.67-1.19 (m, 20H,*Cy*).^{13}CNMR (400 MHz, DMSO-d_6): δ ppm: 207.1 **(-$N^{13}CS_2$)**, 164.4 (*C*=O), 137.0, 136.9 (*C*-N), 129.4, 119.6 (*Ph*), 59.4 (*C*H of *Cy* /NCH_2CO), 48.2 (Ph-CH_2), 29.3, 25.3, 24.8 (CH_2 of Cy).

[Cu_2-μ^2-bis-{(κ^2*S,S*-$S_2CN(Cy)CH_2CONHC_6H_4)_2CH_2$}](1b). Brown; MW: 1380, Yield: 441.3 mg, 64 %; m.p. 208 °C dec.ES-MS: 1381.4 (M+H). FTIR (KBr disc, cm^{-1}):3300.48w, 2932.95vs, 2853.64s, 2099.79w, 1759.17m, 1690.63m, 1603.70s, 1514.53vs, 1453.29vs, 1410.10vs, 1350.05w, 1305.34s, 1240.76vs, 1192.06w, 1164.63m, 1010.42s, 971.55m, 894.89w, 813.97w, 674.19w, 503.97w, 417.84w.

[Zn_2-μ^2-bis-{(κ^2S,S-$S_2CN(Cy)CH_2CONHC_6H_4)_2CH_2$}](1c). Yellow; MW: 1384, Yield: 290.3 mg, 42%; m.p. 212 °C dec. FTIR (KBr disc, cm^{-1}): 3316.58w, 2931.13vs, 2854.91s, 2360.12w, 2096.12w, 1900.78w, 1758.68w, 1690.37vs, 1677.64vs, 1602.98vs, 1515.05vs, 1467.77m, 1451.37s, 1410.34s, 1350.07w, 1306.76s, 1240.69s, 1190.56w, 1164.81s, 1009.28s, 969.82s, 915.04w, 894.31w, 858.40w, 773.59w, 668.18w, 609.52w, 503.62m, 476.07w, 426.09w. ^{1}H NMR (DMSO-d_6, 400 MHz) δ, ppm: 10.02 (s, 4H, CON*H*); 7.45 (d, 8H, *Ph*); 7.11 (d, 8H, *Ph*); 4.62 (s, 8H, NCH_2CO); 3.81 (m, C*H* of Cy); 3.31 (merged with DMSO-d_6, Ph-CH_2);1.66-0.89 (m, 20H, *Cy*).^{13}C NMR(400 MHz, DMSO-d_6) : δ 206.1 **(-N^{13}*C*S_2)**, 165.7 (*C*=O), 137.4, 136.5 (*C*-N); 129.4, 119.5, (*Ph*), 64.1 (*C*Hof*Cy*); 51.9 (N*C*H_2CO); 49.3 (Ph-*C*H_2), 30.0, 29.6, 25.7, 25.1 (*C*H_2 of Cy).

[Ni_2-μ^2-bis-{(κ^2S,S-$S_2CN(^iPr)CH_2CONHC_6H_4)_2CH_2$}] (2a). dark Green; MW: 1210, Yield: 153.6 mg, 82%; m.p. 240 °C dec.ES-MS: 1211.5 (M+H). FTIR (KBr disc, cm^{-1}): 3284.75m, 3187.43w, 3121.71w, 2972.59s, 2906.55m, 2837.62w, 2361.50m, 2092.93br, w, 1761.63w, 1684.48vs, 1603.20s, 1513.99vs, 1468.21vs, 1409.76vs, 1366.08m, 1350.07m, 1305.69vs, 1274.80w, 1245.23vs, 1171.34vs, 1071.27vs, 1010.45s, 969.51s, 907.53m, 814.35m, 773.41w, 648.49m, 575.97w, 501.87m, 456.78w, 421.79w.^{1}H NMR (400 MHz, DMSO-d_6): δ (ppm) 10.13(s,4H,N*H*) ; 7.44-7.11(m,16H,*Ph*) ; 4.65 (NCH_2CO); 4.31 (s, 4H, C*H* of ^{i}Pr); 3.82 (s, 4H, Ph-CH_2), 1.16 (d, 24H, CH_3). ^{13}CNMR (400 MHz, DMSO-d_6) δ ppm: 206.7 **(-N^{13}*C*S_2)**, 164.5 (*C*=O), 137.0, 136.9 (*C*-N); 129.4, 119.6 (*Ph*), 51.4 (N*C*H_2CO); 48.4 (*C*H of ^{i}Pr), 47.9 (Ph-*C*H_2), (*C*H of ^{i}Pr); 19.5, 19.3 (*C*H_3 of ^{i}Pr).

[Cu_2-μ^2-bis-{(κ^2S,S-$S_2CN(^iPr)CH_2CONHC_6H_4)_2CH_2$}] (2b). Dark Brown; MW: 1220, Yield: 329.1 mg, 54%; m.p. 168 °C dec. ES-MS: 1221.4 (M+H). FTIR (KBr disc, cm^{-1}): 3487.87br, w, 3272.23w, 3187.32w, 3030.93w, 2972.87m, 2903.84w, 2380.01w, 2280.53w, 2082.26w, 1870.73w, 1764.39m, 1735.02w, 1684.11vs, 1603.88vs, 1512.92vs, 1463.73vs, 1409.21s, 1365.72m, 1305.14sh, 1248.68m, 1170.42vs, 1070.69vs, 1006.40m, 967.87m, 909.82w, 846.17w, 815.07m, 773.62m, 709.51w, 646.55m, 558.83w, 503.37m, 478.44w, 457.89w, 422.77w.

[Zn_2-μ^2-bis-{(κ^2*S,S*-$S_2CN(^iPr)CH_2CONHC_6H_4)_2CH_2$}] (2c). Pale Yellow; MW: 1224, Yield: 293.4 mg, 48 %; m.p. 175 °C dec. ES-MS: 1225.8 (M+H). FTIR (KBr disc, cm^{-1}): 3514w, 3274.45w, 3187.15w, 3120.78w, 3030.89w, 2973.55m, 2367.59w, 1812.40br, w, 1677.83vs, 1603.73vs, 1512.77vs, 1463.60m, 1453.38w, 1410.56s, 1367.00w,1344.76w, 1306.83s, 1249.53m, 1173.59s, 1127.18w, 1071.65m, 1003.28w, 967.53m, 911.65w, 862.81w, 814.85m, 773.95w, 648.53m, 561.08w, 507.20w, 479.08w, 458.23w, 411.99w, 425.18m. ^{1}H NMR (DMSO-d6, 400 MHz): δ (ppm) 10.03 (s, 4H, CON*H*); 7.45 (m, 8H, *Ph*); 7.09 (m, 8H, *Ph*); 4.49 (s, 8H, NCH_2CO); 4.33 (s, 2H, C*H* of ^{i}*Pr*); 3.81 (m, 2H, Ph-CH_2); 1.23-1.03 (m, 24H, CH_3 of ^{i}Pr). ^{13}C NMR (400 MHz, DMSO-d_6) δ ppm: 208.0 **(-N^{13}*C*S_2)**; 180.9, 171.3, 165.9 (*C*=O); 147.0, 137.5, 136.9 (*C*-N), 129.3, 119.6, 114.4, 114.4 (*Ph*); 55.83 (*C*H of ^{i}Pr); 51.06, 50.27 (N*C*H_2CO); 48.5 (Ph*C*H_2); 22.5, 19.9, 19.5 (*C*H_3 of ^{i}Pr).

[Ni_2-μ^2-bis-{(κ^2*S,S*-$S_2CN(^nBu)CH_2CONHC_6H_4)_2CH_2$}](3a). Dark Green; MW: 1267, Yield: 531.5 mg, 84 %; m.p. 268 °C dec. ES-MS: 1267.5 [M^+]. FTIR (KBr disc, cm^{-1}): 3279.99m, 3123.63w, 3030.11w, 2956.66s, 2928.40m, 2867.48w, 2361.09w, 2344.03w, 2091.92w, 1676.91vs, 1604.19vs, 1508.68vs, 1433.05m, 1409.87s, 1363.64m, 1306.12m, 1275.80w, 1251.86w, 1226.19m, 1173.55m, 1111.96m, 1012.65m, 970.12w, 937.68w, 911.86w, 874.99w, 814.34m, 772.31w, 626.19w, 504.61w, 417.59m. ^{1}H NMR(DMSO-d6, 400 MHz): δ (ppm) 10.15 (s, 4H, CON*H*); 7.44 (d, 8H, *Ph*); 7.12 (m, 8H, *Ph*); 4.40 (s, 8H, NCH_2CO); 3.83 (s, 8H, NCH_2 of ^{n}*Bu*); 3.59 (s, 4H, PhCH_2); 1.56, 1.24 (m, 16H, CH_2 of ^{n}*Bu*) 0.90-0.85 (m, 12H, CH_3 of ^{n}*Bu*). ^{13}C NMR (400 MHz, DMSO-d_6) δ (ppm) 207.1 **(-N^{13}*C*S_2)**, 164.2 (*C*=O), 137.0, 136.9 (*C*-N), 129.4, 119.6 *Ph*), 51.8 (N*C*H_2CO); 51.3 (N*C*H_2 of ^{n}*Bu*); 51.1 (Ph-*C*H_2); 28.7, 19.8 (*C*H_2 of ^{n}*Bu*); 14.0 (*C*H_3 of ^{n}Bu).

[Cu_2-μ^2-bis-{(κ^2*S,S*-$S_2CN(^nBu)CH_2CONHC_6H_4)_2CH_2$}](3b). Brown; MW: 1276, Yield: 414.4 mg, 65%; m.p. 215 °C dec.ES-MS: 1277.4 (M+H). FTIR (KBr disc, cm^{-1}): 3280.46m, 3196.26m, 3122.09w, 3081.38w, 2956.63s, 2928.75s, 2868.44m, 2633.01w, 2359.32w, 2345.71w, 2175.93w, 2111.35w, 1792.19s, 1688.50s, 1670.11vs, 1654.43s, 1604.43vs, 1542.56s, 1522.09s, 1542.56s, 1486.99s, 1430.52s, 1410.95vs, 1363.98m, 1306.09s, 1251.10m, 1224.87s, 1178.88s, 1111.40s, 1011.10s, 972.86m, 937.48w,

912.81m, 858.13w, 814.37m, 772.70m, 731.00w, 668.26w, 625.69w, 505.18m, 442.31w, 417.96m.

[Zn_2-μ^2-bis-{(κ^2*S,S*-$S_2CN(^nBu)CH_2CONHC_6H_4)_2CH_2$}](3c). Yellow; MW: 1280, Yield: 281.3 mg, 44 %; m.p. 223 °C dec. ES-MS: 1281.6 (M+H). FTIR (KBr disc, cm^{-1}): 3286.09m, 3124.54w, 3040.14w, 2957.11s, 2929.56s ,2866.55m, 2358.78m, 2085.51w, 1857.84w, 1857.84w, 1745.54m, 1727.45w, 1672.65vs, 1601.94vs, 1549.83s, 1484.42s, 1431.22m, 1363.87m, 1308.19s, 1251.28m, 1224.30m, 1176.25s, 1113.06s, 1008.45s, 970.15m, 937.27w, 911.79w, 857.57m, 815.31m,773.37m, 732.54w, 621.62w, 555.79w, 503.59m, 442.44w, 417m. ^{1}H NMR (DMSO-d6, 400 MHz): δ (ppm) 9.96 (s, 4H, CON*H*); 7.44 (m, 8H, *Ph*); 7.09 (d, 8H, *Ph*); 4.79 (s, 8H, NCH_2CO); 4.34 (s, 8H, NCH_2 of ^nBu); 3.80 (s, 4H, Ph-CH_2); 1.82-1.74 (m, 16H, CH_2 of ^{n}Bu); 1.35-1.10 (m, 12H, CH_3 of ^{n}Bu).

3.2.4 *In vitro* cytotoxicity studies

3.2.4.1. Cell line and Culture

The hepatoma cancer cell line HEP G2 was procured from the National Centre for Cell Science, Pune whereas Dulbecco's Modified Eagle's Medium (DMEM), Fetal Bovine Serum (FBS) and antimycotic–antibiotic solution were procured from Gibco, Invitrogen and Cisplatin from Sigma Aldrich. The cell line was maintained in DMEM with 10% FBS in humidified atmosphere supplied with 5% CO_2 at 37°C and was utilized to examine the cytotoxic activity of testing compounds at varying concentration.

3.2.4.2 MTT assay for cell viability/ proliferation

The MTT assay was used to determine cell growth inhibition. All the compounds viz. **L'**, **L^1**, **L^2**, **L^3** and their ensuing transition metal dithiocarbamate complexes **1a-1c**, **2a-2c**, **3a-3b** were dissolved in 5% DMSO and then diluted with culture media. Cells were seeded in 96-well plates at a density of 1×10^3 cells per well and incubated for 24hrs after which

they were treated with different concentrations (6.25µg/ml, 12.5µg/ml, 25µg/ml, 50µg/ml and 100 µg/ml) of compounds for 24hrs. Under the similar experimental conditions cisplatin was also screened against HepG2 at different doses. Finally the media was removed and the cells were incubated with 10µL of 5 mg/ml stock solution of MTT in PBS for 4hrs at 37°C in 5% CO_2 incubator. The resultant formazan crystal formed by metabolically viable cells was dissolved by adding DMSO. The optical density was measured at 540nm by an ELISA reader (BIOTEK ELX800 Universal Microplate Reader). [38]

3.2.4.3 Statistical analysis for determination of IC_{50}

Data obtained was analyzed in Prism/OriginPro 8 for standard error and probit analysis. The percent cytotoxicity index (% CI) was calculated as follows:

% CI= [1− (OD of treated cells/ OD of control cells)] × 100 %

where, CI= cytotoxicity index, OD= optical density.

A plot of % CI versus concentration was obtained from the experimental data for each set of experiments. The values of IC_{50} (50% growth inhibition of cell) were determined from the graph.

3.2.4.4 Assessment of apoptosis AO/EtBr staining

Cells were grown in 24 well-plate (5 x 10^5) and were incubated in a CO_2 incubator at 37^0C. Cells were dosed with IC50 concentration of compounds. After 24hrs of incubation, cells were washed with PBS and stained with 200µl of AO-EtBr mixture (100µg/ml AO: 100µg/ml EtBr). Cells were observed under FLoid™ Cell Imaging Station (Life Technologies) fluorescent microscope at 20X magnification. [39]

3.3 Result and Discussion

3.3.1 Syntheses and characterization

The cytotoxic effects of 4,4'-diaminodiphenylmethane (**L**) on hepatocarcinogenes is in male F344 rats[11] and in continuation to our ongoing research interest,[10] three

symmetrical secondary diamine precursors 4,4'-bis(2-(alkylamino)acetamido)diphenylmethane (**L^1-L^3**) were synthesized in >75 % yields by the nucleophilic substitution of α-chloro substituents of 4,4'-bis(2-chloroacetamido)diphenylmethane (**L'**) with a number of primary amines as shown in Scheme 1. The 4,4'-bis(2-(n-butylamino)acetamido)diphenylmethane can also be obtained through 2-bromoacetamide derivative, however it took long duration to complete.[14] **L^1-L^3** are soluble in common organic solvents and stable in solid and in solution state. In contrast to **L^3**, precursors **L^1-L^2** melted beyond 100 °C which are indeed supported by TGA/DTA study. These compounds were satisfactorily characterized by standard spectroscopy.

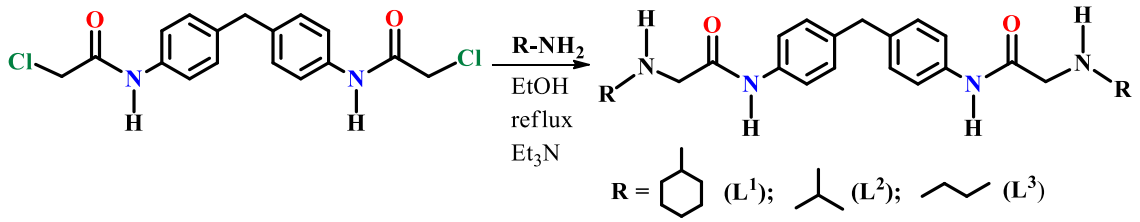

Scheme 1: Preparation of 2° diamine precursors L^1-L^3.

Interestingly, a room temperature single-pot reaction protocol involving self-assembly of the corresponding diamine **L^1-L^3** with CS_2 and transition metal ion viz. Ni^{II}, Cu^{II} or Zn^{II} has led to the formation of a new series of metallomacrocyclic dithiocarbamate complexes **1a-1c, 2a-2c, 3a-3c** in moderate to good yields as illustrated in Scheme 2.

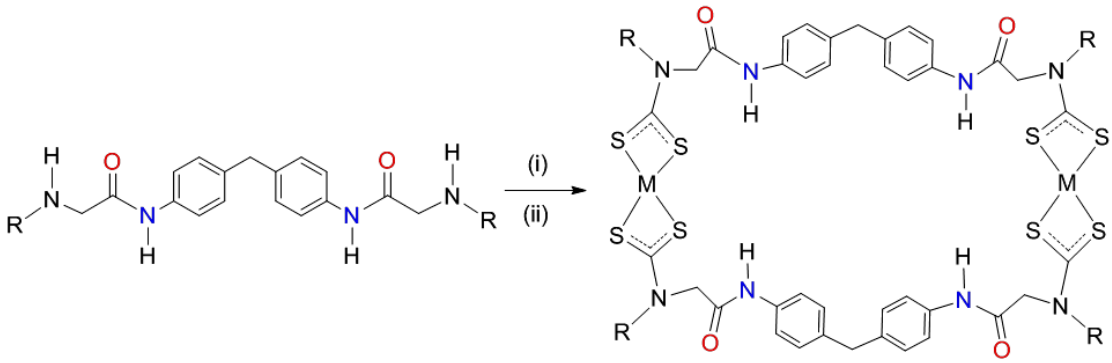

Scheme 2: Single-pot synthetic methodology adopted for metallomacrocyclic dithiocarbamate complexes 1a-1c, 2a-2c and 3a-3c.

It may be noted that the green color (**1a, 2a, 3a**), brown color (**1b, 2b and 3b**) and yellow color (**1c, 2c, 3c**) macrocyclic complexes are insoluble in common organic solvents, however they exhibit good solubility in the solvents of high polarity such as DMF, DMSO.

3.3.2 NMR, Mass and IR spectral study

The ES-MS spectra of $\mathbf{L^1}$-$\mathbf{L^3}$ gave molecular ion peaks at 474.1, 396.4 and 422.3, respectively, which correspond to either [M-2H] or [M^+] along with expected fragments (Annexure 1 and Annexure 4). The characteristic IR bands for $\mathbf{L^1}$-$\mathbf{L^3}$ are appeared in the range of 3470-3100 cm^{-1}, 3042-2851 cm^{-1}, 1689-1666 cm^{-1}, 1606-1526 cm^{-1} and 1410-916 cm^{-1}, attributed to ν(N-H), aromatic ν(C-H), ν(C=O), ν(C=C) and ν(C-N) stretching vibrations respectively. A very strong band in the region of 844-815 cm^{-1} due to the aromatic ν(C-H) suggests the presence of *para*-disubstituted benzene rings in these molecules.[10a] Moreover, the possibility of involvement of amide/amine functionalities of $\mathbf{L^1}$-$\mathbf{L^3}$ in the intermolecular hydrogen bonding in the solid state is revealed by the appearance of a broad or multiple nature of ν (NH) vibration. (Annexure 8 and Annexure 12) The characteristic ^{1}H NMR signals for $\mathbf{L^1}$-$\mathbf{L^3}$ appeared at ~ 9.76 ppm and at ~3.82 ppm due to amide protons (CON*H*) and α-methylene protons (NCH_2CO) respectively

with proper splitting patterns. These signals experienced significantly down-field shifting compared to their positions in analogous compounds. [10b, 10d] A characteristic amine –NH signal could be seen as a broad peak in the range of 2.68-1.7 ppm. The methylene/ methine protons and other signals corresponding to the protons of aromatic and N-alkyl substituents are appeared in the expected range as multiplets due to coupling with adjacent protons. The characteristic ^{13}C NMR signals are appeared in the range of 171-170 ppm, 50-59 ppm and 48-56 ppm due to carbonyl, the α-methylene (NCH_2CO) and aliphatic *N*-substituents (N*C*H/ N*C*H_2) respectively. The assignments of ^{13}C NMR signals for **L^1-L^3** are supported by DEPT-135 experiment.(Annexure 16-27) The metallomacrocyclic dithiocarbamate complexes (**1a-1c, 2a-2c** and **3a-3c**) were sufficiently characterized by various spectroscopic techniques viz. ESI-MS, FTIR, NMR (^1H, ^{13}C, DOSY), UV-visible. The experimental data are further validated by DFT level calculations performed on representative compounds. The ESI-MS spectra of these complexes gave m/z molecular ions peaks at 1372.8, 1381.4, 1211.5, 1221.4, 1225.8, 1267.5, 1277.4, and 1281.6 for 1a, 1b, 2a, 2b, 3a, 3b, 3c, respectively which corresponds to either [M+H] or [M^+] molecular ions. (Annexure 2, 3, 5, 6 and Annexure 7) The IR spectra of these complexes show the ν(C–N) and ν(C–S) frequencies at 1486–1408 and 1071–967 cm^{-1} respectively characteristic of the dithiocarbamate ligand coordination. Besides, a medium to weak intensity ν(M-S) bands are observed in the 503-417 cm^{-1} range which is in agreement with the earlier observations.[15] (Annexure 9, 10, 11, 13, 14 and Annexure 15) The composition and purity of all the complexes have been confirmed by characteristic ^1H and ^{13}C , DOSY NMR signals. The ^1H NMR spectra of the complexes (ESI) show the presence of ligand functionalities and fit in well to the corresponding hydrogen. In the ^{13}C NMR spectra, all complexes show a single downfield resonance at δ 208–206 ppm associated with the N–CS_2 unit. [10] (Annexure 29, 32, 34 and Annexure 37) Besides, a significant shifting of $^1H/^{13}C$ signals associated with *N*-methylene, *N*-methine and $PhCH_2$- in the complexes, compared to those of the free diamine precursors toughen the formation of proposed structures as they are most sensitive to any kind of chemical change at amine functionality. The coordination driven self-assembly of a discrete molecular structure depends on the stereo-electronic features of ligand framework, metal centers as well as thermodynamic conditions.[16] Moreover,

because of the high conformational freedom associated with bridging group (–$C_6H_4CH_2C_6H_4$-/ –$C_6H_4SO_2C_6H_4$-), the bis-*N,O*-bidentate Schiff-base ligands derived from 4,4'-diaminodiphenylmethane/ 4,4'-diaminodiphenylsulfone evidently bind two metal ions separately leading to the formation of binuclear macrocyclic self-assembly.[17] The ^{1}H DOSY NMR spectral analysis of complexes 1a (Annexure 30), 1c (Fig. 1), 2a (Annexure 35) and 3a unambiguously display the presence of only one type of species in solution and rule out the possibility of formation of oligomers or coordination polymers.

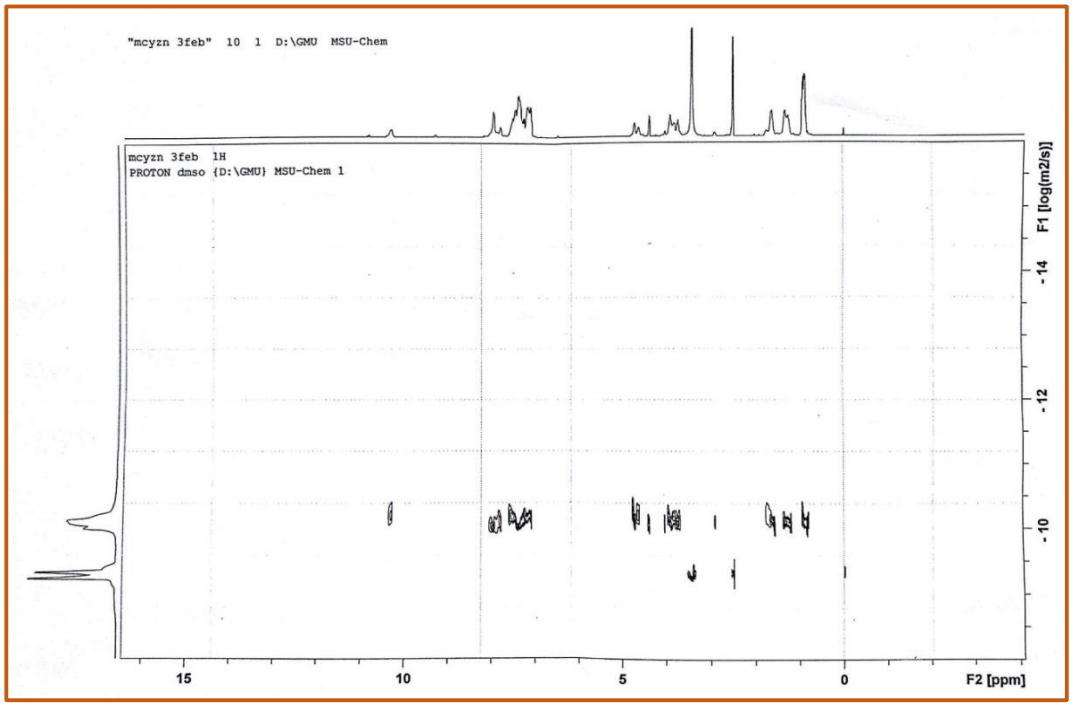

Fig. 1. DOSY NMR spectrum of 1c.

3.3.3 UV-visible absorption, magnetic moment and fluorescence emission study

The UV-visible absorption spectra of **L^1-L^3** exhibit a single noticeable band at shorter wavelength at ~300 nm assignable to π→π* (phenyl) transitions. All the diamagnetic complexes show three foremost bands in the region of 301-326; 348-392 and 432-485nm, attributable to intra-ligand π→π*, n→π* and L→M charge-transfer transitions, respectively (Annexure 38-40) and Table 1. Such lower energy charge-transfer transitions are reportedly caused by the electron withdrawing nature of the amide groups.[18] As expected, copper complexes **1b, 2b** and **3b** display additional band in the region of ~ 629-653 due to d-d transition, apart from the bands due to π→π* and L→M charge-

transfer transitions. The NMR, magnetic moment values, along with UV-visible absorption bands suggest square planar/distorted square planar environment around Ni^{II}/ Cu^{II} centers and tetrahedral/distorted tetrahedral environment around Zn^{II} centers in their respective complexes [10d, 19] which is further supported by DFT study.

Table 1

UV-visible absorption, magnetic moment and fluorescence data for the compounds

Entry	UV-visible spectral data (10^{-3} M DMF)	Wave number	Magnetic Moment	Fluorescence spectral data (10^{-3} M DMF)	
	λ_{max} nm (ε, $LMol^{-1}cm^{-1}$)		μ_{eff}(BM)	λ_{ex} nm	λ_{em}(nm) (Intensity)
L^1	302 (14113) π→π*	3311	-	302	351 (449) π*→π
L^2	300 (301.7) π→π*	3333	-	300	430 (29)
L^3	301 (557.5) π→π*	3322	-	301	350 (23) π*→π
1a	325 (56954) π→π*; 390 (10369) n→π*; 480(1222) charge transfer	3076, 2564 2083	dia	---	Non fluorescent
1b	301 (6318.7) π→π*; 438 (4971.1) charge transfer 629 (629.05) *d-d transition*	3322 2283 1589	1.90	301	352 (13)
1c	301 (6259) π→π*; 348 (1860.5) n→π*; 462(192.5)charge transfer	3322,2873 2164	dia	301	430(29) π*→π
2a	326 (71740) π→π*; 392 (1289) n→π* 485(1210) charge transfer	3067, 2551 2061	dia	---	Non Fluorescent
2b	301 (9169.6) π→π* 440 (10166) charge transfer 653 (810.8) *d-d transition*	3322 2272 1531	1.87	---	Non fluorescent
2c	302 (3869.2) π→π*; 354 (871.6) n→π*; 432 (484.3) charge transfer	3311,2824 2314	dia	---	Non fluorescent
3a	325 (66960) π→π*; 392 (13220) n→π*, 484 (2100) charge transfer	3076, 2551 20661	dia	---	Non Fluorescent
3b	302 (6228) π→π* 440 (7003) charge transfer 650 (559) *d-d transition*	3311 2272 1538	1.89	---	Non Fluorescent
3c	301 (3250) π→π*; 349 (736.7) n→π*; 454 (700) charge transfer	3322, 2865 2202	dia	305	400 (2) π*→ π

Notably molecule that provides intense absorption enables the designing of luminescent compounds as a possible molecular biological probe in human cells, tissue, and organisms. [20] Thus all the newly synthesized compounds were studied for their fluorescence properties.

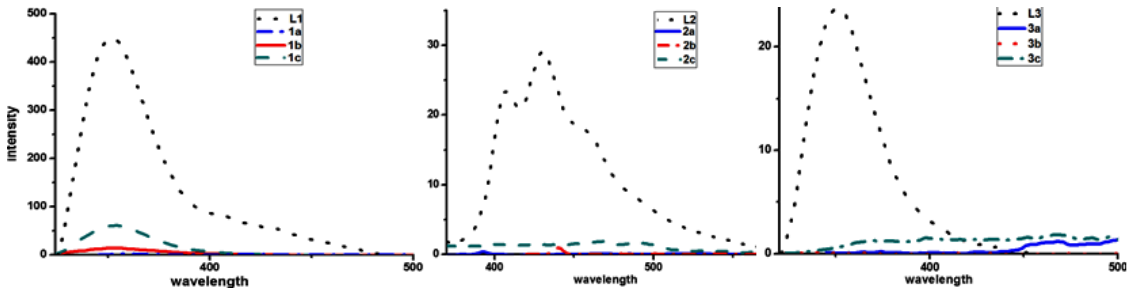

Fig. 2. Fluoresecence emmission spectra of L^1-L^3 and their metallomacrocyclic dithiocarbamate complexes 1a-1c, 2a-2c and 3a-3c in DMF solution.

Reportedly, transition metals are good fluorescence quenchers because their complexes with fluorescent ligands are paramagnetic and contain unpaired metal *d* electrons.[10c, 21] Consequently, Zn(II) [20a, 22] and other transition metals [23] with d^{10} configurations are well known fluorescence intensifier, however many of the diamagnetic Ni(II) complexes with square planar geometry have appeared as fluorescence quenchers at several occasions [21] and their quenching rates [24] are found above 10^{10} dm^3 mol^{-1} s^{-1}.

At present case, ligand precursors 4,4'-bis(alkylamino)acetamido)diphenylmethane evidently fluoresces at 302, 430 and 350 nm from locally excited $\pi \rightarrow \pi^*$ transition states with concomitant Stoke shifts of 49, 130 and 49 nm, respectively (Fig. 2). This fluorescence is successfully quenched by Ni^{II}/ Cu^{II} and by Zn^{II} ions in their corresponding dithiocarbamate complexes 1a-1c, 2a-2c and 3a-3c. The unusual fluorescence quenching behavior of Zn^{II} ions in their metallomacrocyclic dithiocarbamate complexes may be attributed to the dominant photo induced electron transfer process upon complex formation. [25] Besides literature reports suggest that the fluorescence properties of the compounds greatly depends upon the molecular arrangements, achieved by means of polymorphism, conformational stiffness of the fluorophore (dihedral angles), intermolecular interactions such as $\pi \ldots \pi$ or C-H$\ldots\pi$ interactions and upon the nature of substituents which can largely affect the photo induced electron transfer processes.[26]

3.3.4 Thermogravimetric study

Thermogravimetric plots of L^1-L^3 and their metal complexes 1a-1c, 2a-2c and 3a-3c obtained under N_2 atmosphere from room temperature to 550 °C at a heating rate of 10 °C/min along with the temperature ranges corresponding to percentage weight loss, varied rate of decompositions, and stable residual mass (Annexure 41-43) Notably, a multi stage thermal degradation patterns were observed on TG curves for all the compounds except for **L^1-L^3, 1b, 3a** (a single stage). It may be noted that **L^1-L^3** exhibit first endothermic peak at 134.1 °C, 106 °C and 45 °C, respectively on DTA curves without any significant mass loss on corresponding TG curves. This may be due to the phase change attributable to the melting points of respective compounds. However, thermal decompositions of all metal complexes start before their melting points and accompanied by the appearance of one or more endothermic peak on corresponding DTA curves. Amongst the metal complexes, complexes **1c, 2a** and **3c** are thermally unstable and their degradations start at a lower temperature (< 100 °C), however other compounds are apparently thermally stable up to 150 °C (ESI). Despite of the similar type of molecular framework, the assortment in the thermal degradation pattern of these compounds could be attributed to the possible intermolecular interactions in the solid state. The overall data is consistent with the earlier reports on thermal decomposition of transition metal (II) dithiocarbamate complexes. [27]

3.3.5 Geometry Optimization

A full geometry optimization of some representative compounds viz. diamine precursor **L^1** and its complexes **1a-1c** (Fig. 3) has been performed by using density functional theory (DFT) at B3LYP/6-31G (d, p) and B3LYP/LanL2DZ basis sets, respectively to have better understanding of experimental results. Calculations were performed using the Gaussian 03 program suite [28] and molecular orbitals were generated by Gauss View 3.0 program. Similar calculations have been used in recent years to provide reasonably good results for large molecular structures.[29] The structural parameters (selected bond lengths and bond angles) of complexes **1a-1c** (Table 2) are found to be consistent with the similar parameters deduced experimentally for analogous compounds [30a-30c] by means of single

crystal XRD and require no further comment. The trans annular M···M distances fall in the expected range when compared with the similar distances calculated for analogues systems. [10, 19a] The DFT study confirms the existence of diversified *'gauche'* conformation of both the internal phenyl groups, loss of coplanarity of amide groups and substantial deviations in the Ar-CH_2-Ar angles amongst L^1 and its dithiocarbamate complexes **1a-1c** (Table 2). For instance, the normal Ar-CH_2-Ar bond angle of 116.70Å determined experimentally [31] for the lead compound 4,4'-diaminodiphenylmethane (L) decreases significantly to 114.38 Å in L^1 which indeed further decreases to 108.88-111.06 Å (Table 2) upon the formation of corresponding dithiocarbamate complexes **1a-1c**. The flexibility associated with –$(CH_2CONHC_6H_5)_2CH_2$– linker framework of the ligand precursors would be an important factor; not only responsible for the formation of macrocyclic structure but also for their effective interactions with biomolecules. The optimized geometries of **1a-1c** (Fig. 3) clearly suggest the formation of complexes having distorted square planar geometry around nickel(II)/ copper(II) centres and distorted tetrahedral geometry around zinc(II) centre in **1a-1c** complexes respectively which is consistent with the spectroscopic results. The appearance of almost similar M-S bond distances in the range of 2.25-2.29 Å, 2.37-2.40 Å and 2.43-2.45 Å for nickel(II) **1a,** copper(II) **1b** and for zinc(II) **1c** complexes suggests an isobidentate coordination modes of the -NCS_2 moieties, respectively. Further, spacefilled representation of the optimized geometry clearly reveals a cavity generated by the metallomacrocyclic dithiocarbamate complexes **1a-1c** (Fig. 4).

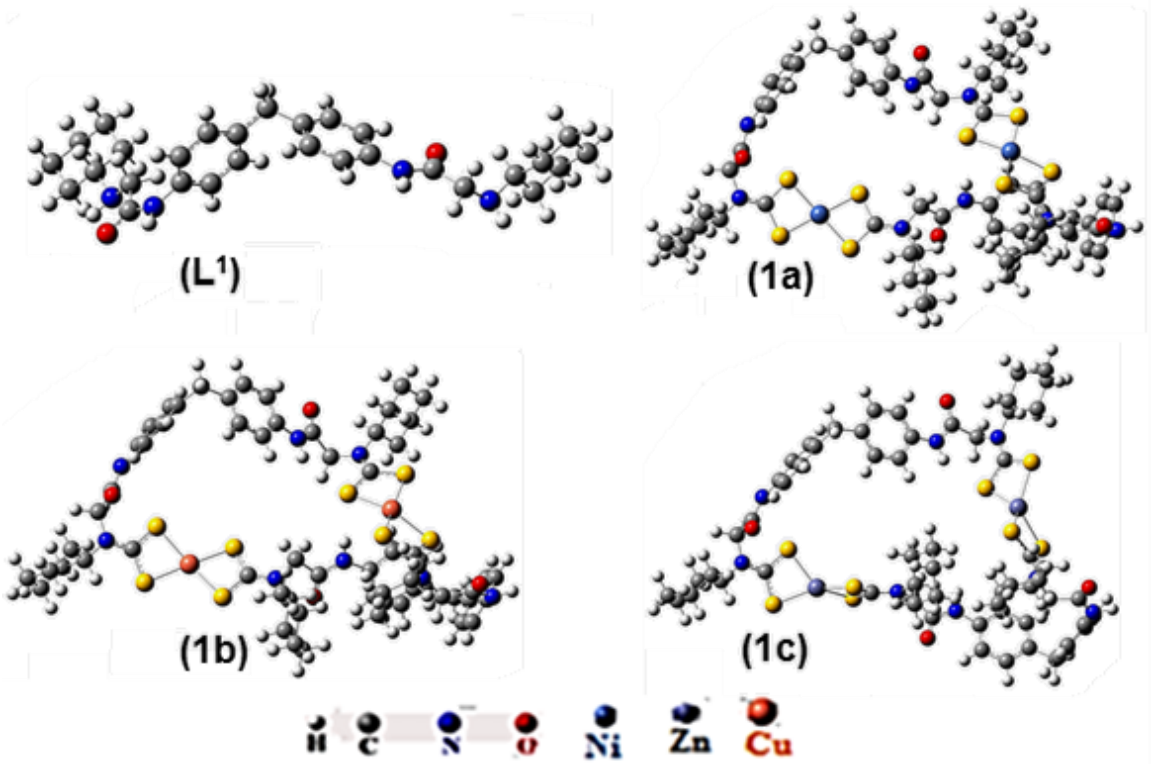

Fig. 3. An optimized geometry for the minimum energy conformation for **L¹** and its dithiocarbamate complexes **1a-1c** at (B3LYP/6-31G (d, p)and B3LYP/LanL2DZ levels, respectively.

Table 2
X-ray crystallographically determined bond lengths (Å) and bond angles (°) for analogues Ni^{II} based dithiocarbamate macrocycle,[30a] Cu^{II} based dithiocarbamate macrocycle[30b], Zn^{II} based dithiocarbamatemacrocycle[30c] and computed values for complexes 1a, 1b and 1c.

Parameters	**1a[x]**	**1b[x]**	**1c[x]**
N—C	1.28 -1.50 [30a] 1.33-1.34	1.318-1.328[30b] 1.33-1.34	1.333-1.363[30c] 1.34
C—S	1.69-1.74[30a] 1.72-1.75	1.719-1.727[30b] 1.73-1.76	1.717-1.782[30c] 1.74-1.76
M—S	2.16-2.22[30a] 2.25-2.29	2.288-2.301[30b] 2.37-2.40	2.32-2.44[30c] 2.43-2.45
Transannular M-M	9.950	10.193	11.744
S—M—S (chelate)	78.99-79.87[30a] 77.87-78.25	77.59[30b] 74.94-75.34	79.5-81.2[30c] 75.07-75.86
S—M—S	100.31-177.14 [30a] 100.77-104.10	101.72-103.48[30b] 104.39-111.82	126.53-136.00[30c] 120.25-138.66
C-CH_2-C	109.03, 108.88	109.16, 109.90	111.06, 113.38

[x] Computed values for the metallomacrocycles **1a**, **1b** and **1c** are shown beneath the experimental observed values.

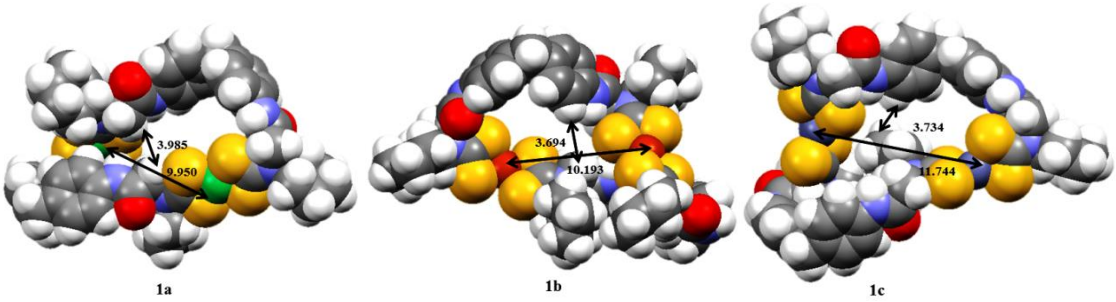

Fig.4. Spacefilled representation of the optimized geometry revealing a cavity generated by the macrocyclic architecture of metallomacrocyclic dithiocarbamate complexes **1a-1c**.

One of the crucial factor for prediction of the properties and potential sites related to the reactivity in biological systems and processes is the molecular electrostatic potential (MESP) of chemical species.[10a,19a] Occurrence of slight negative potential around amide oxygen in addition to positive potential around amide proton is apparent in the mapping of electrostatic potential surface of complexes **1a-1c** (Fig. 5). (Red and blue colour symbolizes localization of negative and positive potential respectively). The localization of negative potential is observed around the metal center in complex **1a** whereas, in case of complex **1b** and **1c** a positive potential around metal centers could clearly be revealed from mapping of electrostatic potential surface (Fig. 5). The polar amide subunits of **1b** and **1c** are indeed projected towards the peripheral side of the macrocyclic motifs (Fig. 5). This can offer H-bond donor-acceptor sites to facilitate the interactions with biomolecules, leading to the effective cellular membrane transportation causing increased concentration of complexes at the site of action.

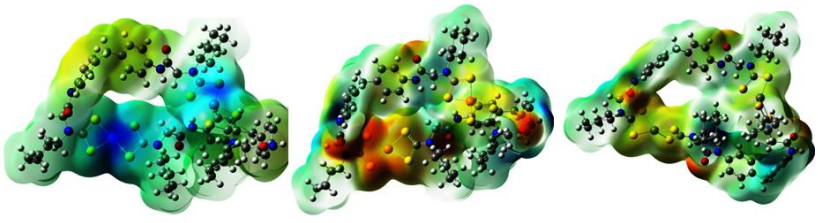

1a **1b** **1c**

Fig. 5. Representations of electron density from total SCF density (Isovalue= 0.0004; mapped with ESP).

Frontier molecular orbital analysis

The calculated HOMO-LUMO energy gaps (Isovalue = 0.02) for ligand precursor **L**[1] and its metallomacrocyclic dithiocarbamate complexes **1a-1c** are given in Table 3 and their localization is illustrated in Fig. 6.

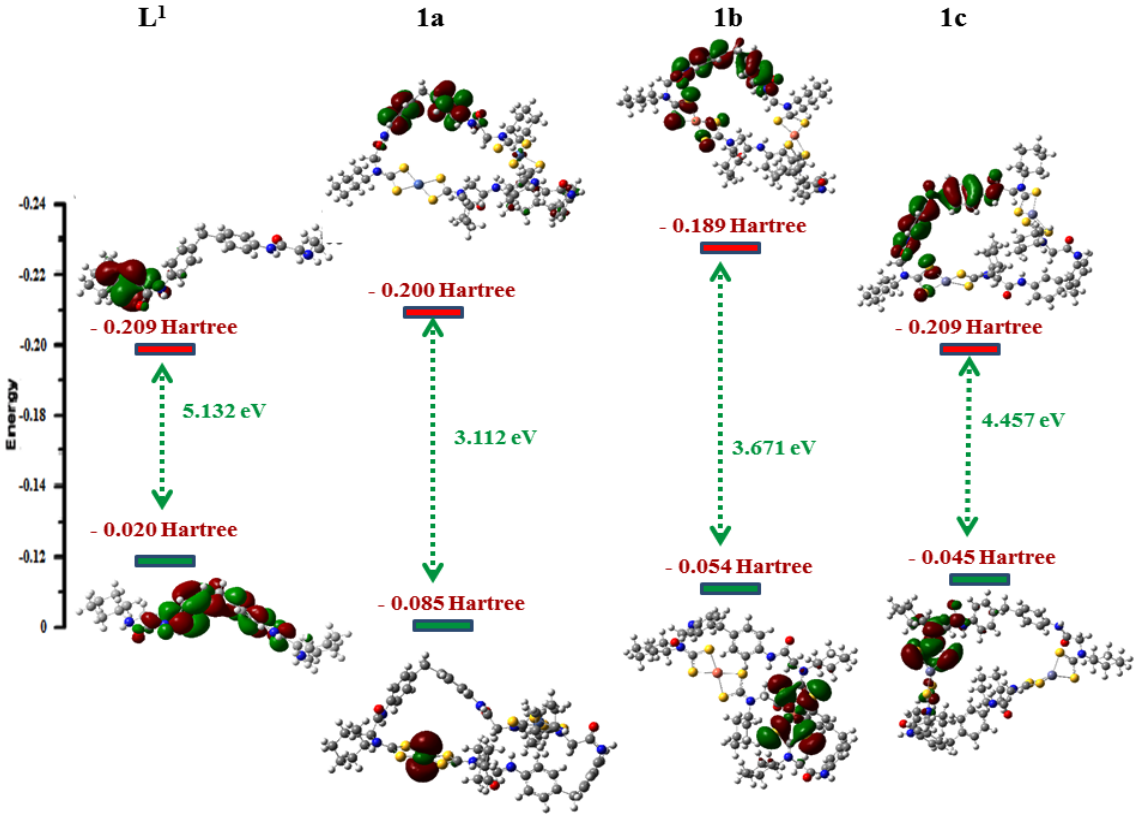

Fig. 6. Frontier molecular orbitals (Isovalue= 0.02) derived from DFT calculation at B3LYP/6-31G (d, p) level: for **L**[1]and at B3LYP/LAN2DZ level: for **1a-1c.**

Table 3
Summary of computational studies performed on L^1 and **1a-1c**

Entry	Energy of optimized geometry (Hartree)	E_{HOMO}, E_{LUMO} (Hartrees)	$\Delta E_{HOMO-LUMO}$ (eV)	λ_{max} calc. (expt.) nm
L^1	-1498.738	- 0.209, - 0.020	5.132	241 (303)
1a	-6671.663	- 0.200, - 0.085	3.112	398 (390)
1b	-6725.322	- 0.189, - 0.054	3.671	337 (301)
1c	-6464.239	- 0.209, - 0.045	4.457	278(301)

The HOMO of $\mathbf{L^1}$ is delocalized over one of the peripheral amide group and LUMO is predominantly located on the π-system of phenyl rings. Contrarily the LUMO in complex **1a** is primarily located at one of the Ni^{II} center (Fig. 6) whereas this molecular orbital in other complexes is delocalized over one of the MCS_2 moiety. This enriches the Lewis acidic character of the cavity. The HOMO of **1a** is primarily delocalized over both the phenyl rings of one linker. The absence of the electron density over the amide group probably decreases the possibility of H-bond formation and reduces the interactions with biomolecules. This explains the poor cytotoxicity of this compound (IC_{50} = 26.3 ± 0.02) of **1a** compared to **1b-1c**. Whereas, in **1b** and **1c** the HOMO is delocalized over the amide groups and the π-system of phenyl rings of one linker explaining the excellent bioactivity of these compounds [IC_{50} = 9.54 ± 0.02 **1b** and IC_{50} = 6.92 ± 0.02 **1c**]. The theoretical parameters correlate well with the experimental results and explain the potency of binuclear complex **1b** and **1c** as effective cytotoxic agents. The λ_{max} values obtained by computational study are comparable with the λ_{max} values (Table 3) determined experimentally by means of UV-visible absorptions which further validate the computational investigations.

3.3.6 *In vitro* cytotoxic activity

Cytotoxic ability of these synthesised complexes was studied *in vitro* against human hepatocellular carcinoma cell line Hep G2 (Hepatoma) by MTT assay. We have selected Hep G2 cell line for investigation because this cell is commonly used as a model system for studies of liver metabolism and xenobiotics toxicity.[32] Hepatocytes are responsible for the breakdown and modification of toxic substances and medicinal products by drug metabolism thus making them major site of detoxification of exogenous and endogenous compounds. Moreover, inhibitory effects of 4,4'-diaminodiphenylmethane on hepatocarcinogenesis have been studied *in vivo* in rats wherein animals were administered 4,4'-diaminodiphenylmethane for 24 weeks post tumor induction, following which the liver tumor incidence was found to be significantly lower compared to control group which indicates the cytotoxic potential of this compound.[33,11] These observations led us to screen newly synthesized derivatives of 4,4'-diaminodiphenylmethane for their possible *in vitro* cytotoxic activity by MTT assay against the malignant tumor cell line Hep G2 (Hepatoma).

The cytotoxicity observed for these compounds were compared with the standard drug cisplatin [C]. The 50% inhibition concentration (IC_{50}) values obtained after incubation for 24hrs for all the compounds against said cell lines are summarized in Table 4 and Fig. 7. Further, complexes exhibiting lower IC_{50} (**L', L^1, 1b, 1c, L^2, L^3** and **3a**) than standard drug were tested on normal liver cell line (WRL-68) under similar conditions.

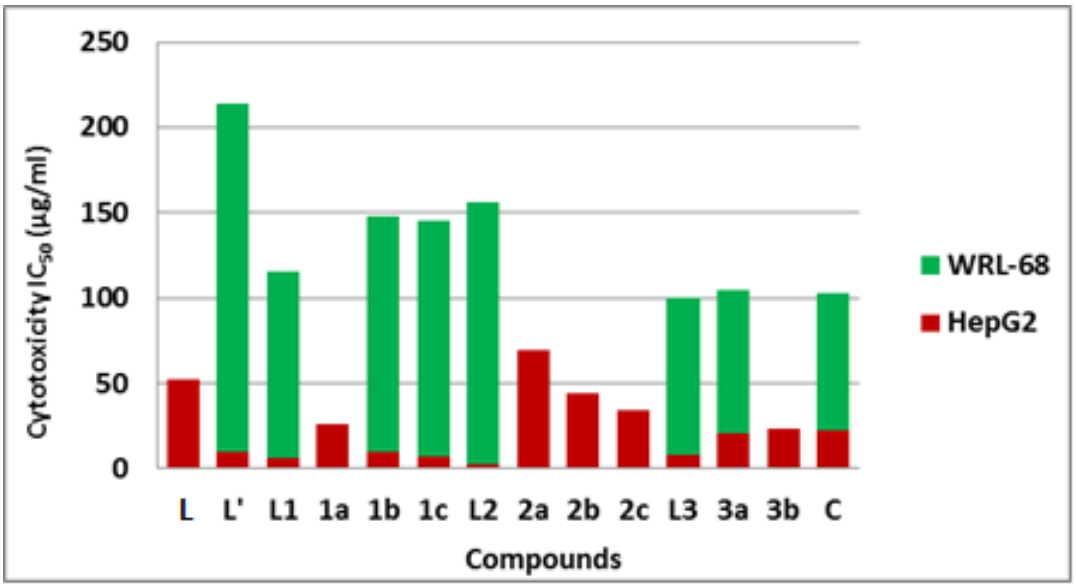

Fig. 7. Cytotoxic activity IC_{50} values (µg/ml) for **L** and its derivatives **L'**, **1a-1c**, **2a-2c** and **3a-3c**.

Table 4
IC_{50} values for entry1-15 against Hep G2 and WRL-68 cell lines.

Entry	Compounds	Cytotoxicity IC50 (µg/ml) ± SE	
		Hep G2	WRL-68
1	4,4'-diamino diphenylmethane (L)	52.48 ± 0.02	-
	4,4'-bis(2-chloroacetamido)diphenylmethane (L')	10 ± 0.06	204.20 ± 0.058
	4,4'-bis(2-(cyclohexylamino)acetamido)diphenylmethane (L^1)	6.62 ± 0.05	109.2 ± 0.053
2	4,4'-bis(2-(isopropylamino)acetamido)diphenylmethane (L^2)	2.95 ± 0.03	153.60 ± 0.063
3	4,4'-bis(2-(n-butylamino)acetamido)biphenylmethane (L^3)	7.94 ± 0.02	92.17 ± 0.061
4	[Ni_2-μ^2-bis-{(κ^2S,S-$S_2CN(Cy)CH_2CONHC_6H_4)_2CH_2$}] (1a)	26.3 ± 0.02	-
5	[Cu_2-μ^2-bis-{(κ^2S,S-$S_2CN(Cy)CH_2CONHC_6H_4)_2CH_2$}] (1b)	9.54 ± 0.02	138.60 ± 0.15
6	[Zn_2-μ^2-bis-{(κ^2S,S-$S_2CN(Cy)CH_2CONHC_6H_4)_2CH_2$}] (1c)	6.92 ± 0.02	138.18 ± 0.10
7	[Ni_2-μ^2-bis-{(κ^2S,S-$S_2CN(^iPr)CH_2CONHC_6H_4)_2CH_2$}] (2a)	69.18 ± 0.02	-
8	[Cu_2-μ^2-bis-{(κ^2S,S-$S_2CN(^iPr)CH_2CONHC_6H_4)_2CH_2$}] (2b)	43.93 ± 0.04	-
9	[Zn_2-μ^2-bis-{(κ^2S,S-$S_2CN(^iPr)CH_2CONHC_6H_4)_2CH_2$}] (2c)	34.60 ± 0.02	-
10	[Ni_2-μ^2-bis-{(κ^2S,S-$S_2CN(^nBu)CH_2CONHC_6H_4)_2CH_2$}] (3a)	20.40 ± 0.04	84.30 ± 0.14
11	[Cu_2-μ^2-bis-{(κ^2S,S-$S_2CN(^nBu)CH_2CONHC_6H_4)_2CH_2$}] (3b)	23.90 ± 0.04	-
15	Cisplatin (C)	22.7±0.025	>80[33]

Interestingly, many of the synthesized compounds showed better activity than the reference drug cisplatin and specificity for cancer cells over normal liver cells (Fig. 7, Table 4). In fact, the first derivative **L'** exhibits more than two fold better activity (52.48 ± 0.02 µg/mL) than the reference drug which is further augmented upon formation of $\mathbf{L^1}$, $\mathbf{L^2}$ and $\mathbf{L^3}$ derivatives (Table 4). Remarkably, ligand precursor $\mathbf{L^2}$ holding *N*-^{i}Pr substituents shows nearly 7 fold better cytotoxic activity against Hep G2 cell line (2.95 ± 0.03 µg/mL), compared to the reference drug cisplatin (22.7±0.025 µg/mL) whereas 2-3 fold better activity is observed for **1b** and **1c**. It may be noted that, the activity of **L'** is upheld upon the formation of $\mathbf{L^1}$-$\mathbf{L^3}$ however the activity of these compounds falls down significantly after further derivatization into corresponding transition metal dithiocarbamate complexes, except complex **1c**. The enhanced cytotoxicity of above mentioned derivatives against Hep G2 cell line opens the window for further testing on other cell lines in future.

Apoptosis is a genetically regulated programmed cell death that controls the development of multicellular organisms by maintaining cell populations in tissues, regulating immune system and aging. Basic oncology research highly focuses on genes and signals regulating apoptosis. The efficacy of cytotoxic drugs is measured by their ability to selectively promote apoptosis in cancer cells while causing less or no damage to normal healthy cells[3,34] The shrinking of cells, a characteristic apoptotic sign,[35] indicating the induction of apoptosis as part of the mechanism of action of these compounds can be clearly visualized by acridine orange/ethidium bromide (AO/EB) staining (Fig. 8) which marks nuclear changes and differentiates between viable, apoptotic and necrotic cells. Compounds viz. **L'**, $\mathbf{L^1}$, **1b**, **1c**, $\mathbf{L^2}$, $\mathbf{L^3}$ and **3a** exhibiting lower IC_{50} values than cisplatin were stained for AO/EB wherein viable cells are stained by AO and show green fluorescence whereas apoptotic cells are stained by EB and show orange to red fluorescence with condensed chromatin. [36] Contrary to our earlier results. [10d] we did not find DNA fragmentation for the above mentioned compounds, while the same showed clear cytotoxicity in AO/EB staining. The induction of apoptosis is further supported by morphological investigations carried out by using microscopic photographs of Hep G2 upon 24 h exposure to the potent compounds and standard cisplatin at their respective *in*

vitro IC_{50} values (Fig. 9). The microscopic photographs clearly differentiate the normal proliferation of cells without any insult (control) from fewer proliferations of cells upon exposure of compound such as **L'**, **L^1-L^3**, **1b**, **1c** and **3a**. These observations thus needs further investigation to elucidate the exact mechanism and pathway of apoptosis being followed.

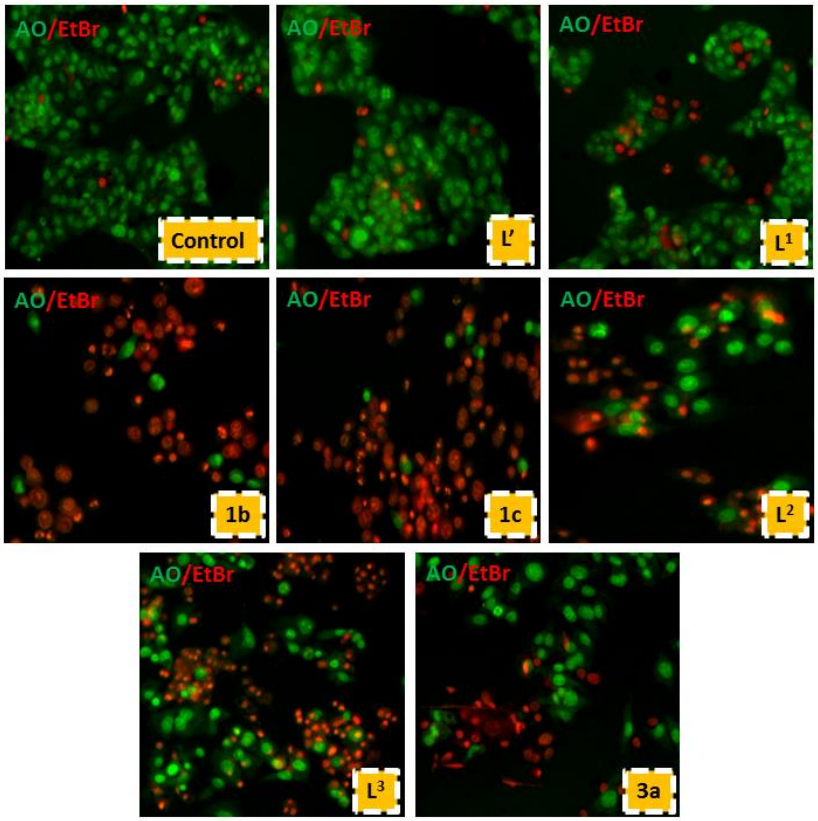

Fig. 8. Acridine Orange (AO)-Ethidium Bromide (EB) staining for detection of live and Apoptotic cells-Green denotes live cells with AO stained cells while red dented apoptotic cells stained with EB

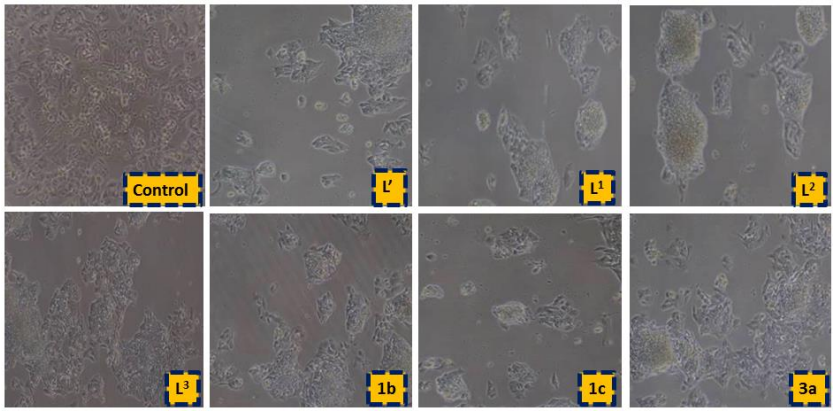

Fig. 9. Phase Contrast images of Hep G2 cells exposed to the potential compounds **L'**, **L^1-L^3**, **1b**, **1c** and **3a** compared to the control indicating the *in-vitro* cytotoxic activity. These compounds were assayed at their respective *in-vitro* growth inhibitory IC_{50} value, as determined using the MTT assay in Hep G2 cells.

3.3.7 Electrochemical study

The electrochemical analysis was performed by using anhydrous solutions of **L^1-L^3** and the metal complexes in dimethylformamide (1.0 mM) containing n-Bu_4NPF_6 (5 mM) as supporting electrolyte at a scan rate of 0.05 Vs^{-1} in the potential ranges +1.5 to -1.5 V. The experiments were carried out with a one-compartment cell having a platinum-disk working electrode, a platinum-wire counter electrode and an Ag/Ag+ (in DMF) reference electrode. All solutions were purged with N_2 for 30 min prior to each set of experiments**.** It appears that all complexes (except **1b, 2b** and **3b**) are primarily electro active with respect to the coordinated ligands and the metal centers are present in silent mode as they did not display any additional peak, compared to the cyclic voltammograms of **L^1-L^3** in the cathodic or anodic scan under the similar experimental conditions. As expected, the cyclic voltammogram of copper complexes displays additional peak in the cathodic/anodic scans in positive potential range due to the formation of Cu^{II}/Cu^{I} redox couples which apparently corresponds toa quasi-reversible process [37d] taking place at copper center.

3.4 Conclusion

In continuation to our ongoing research interest in developing potential metal-based drugs[10] with reduced toxicity and also in the light of observed cytotoxic effects of 4,4'-diaminodiphenylmethane on hepatocarcinogenesis in male F344 rats, we have attempted to derivatise 4,4'-diaminodiphenylmethane into three novel 2° diamines and their ensuing metallomacrocyclic dithiocarbamate complexes (vide supra). All the compounds were structurally characterized by FT-IR, MS, ^{1}H, ^{13}C, ^{1}H DOSY NMR spectroscopy, UV-visible, fluorescence spectrophotometers and by thermogravimetric analysis. The geometry of the compounds has been optimized by density functional theory and electrochemical responses have also been investigated. Fluorescence study reveals an unusual fluorescence quenching behavior of Zn^{II} ions in its corresponding ZnII-dithiocarbamate complexes 1c, 2c and 3c. All the newly synthesized compounds were screened for their *in vitro* cytotoxic activity against malignant human tumor Hep G2 (hepatoma) cell line by the MTT assay. Clearly the first derivative of the lead compound **L'** and its diamino derivatives $\mathbf{L^1}$-$\mathbf{L^3}$ in their metal-free form and their metallomacrocyclic complexes **1b, 1c** and **3a** exhibit higher cytotoxicity than cisplatin. Remarkably, ligand precursor $\mathbf{L^2}$ shows nearly 7 fold better cytotoxic activity against Hep G2 (2.95 ± 0.03 µg/mL) cell line, compared to the reference drug cisplatin. The notable cytotoxic activity of many of the derivatives opens the scope for further investigations against other carcinoma human cell types. The shrinking of cells indicating the induction of apoptosis as part of the mechanism of action of these compounds can be clearly visualized by acridine orange/ethidium bromide (AO/EB) staining which is further supported by morphological investigations. These observations thus need further investigation to elucidate the exact mechanism and pathway of apoptosis.

3.5 References

[1] (a) R. Kieltyka, P. Englebienne, J. Fakhoury, C. Autexier, N. Moitessier and H. F. Sleiman, *J. Am. Chem. Soc*., 2008, 130, 10040. (b) E. M. Driggers, S. P. Hale, J. Lee and N. K. Terrett, *Nat. Rev. Drug Discov*., 2008, 7, 608. (c) J. Mallinson and I. Collins, *Future Med. Chem*., 2012, 4, 1409.

[2] (a) K. N. Burger, R. W. Staffhorst, H. C. de Vijlder, M. J. Velinova, P. H. Bomans, P. M. Frederik and B. de Kruijff, *Nat. Med.*, 2002, 8, 81. (b) Z. Yang, X. Wang, H. Diao, J. Zhang, H. Li, H. Sung and Z. Guo, *Chem. Commun*., 2007, 3453. (c) N. J. Wheate, A. I. Day, R. J. Blanch, A. P.Arnold, C. Cullinane and J. G. Collins, *Chem. Commun.*, 2004, 1424. (d) C. Sanchez-Cano and M. J. Hannon, *Dalton Trans.*, 2009, 10702. (e) A. M. Krause-Heuer, N. J. Wheate, M. J. Tilby, D. G. Pearson, C. J. Ottley and J. R. Aldrich-Wright, *Inorg. Chem*., 2008, 47, 6880.

[3] (a) S. Kemp, N. J. Wheate, M. P. Pisani and J. R. Aldrich-Wright, *J. Med. Chem*., 2008, 51, 2787. (b) N. J. Wheate, *J. Inorg. Biochem*., 2008, 102, 2060.

[4] (a) J. Mallinson and I. Collins, *Future Med. Chem*., 2012, 4, 1409. (b) Mann A. Conformational restriction and/or steric hindrance in medicinal chemistry. In: *The Practice Of Medicinal Chemistry*, Wermuth CG (Ed.). Academic Press, London, UK 2008.

[5] (a) Y. W. Jung and S. J. Lippard, *Chem. Rev*., 2007, 107, 1387. (b) S. K. Singh, S. Joshi, A. R. Singh, J. K. Saxena and D. S. Pandey, *Inorg. Chem*., 2007, 46, 10869. (c) R. K. Gupta, R. Pandey, G. Sharma, R. Prasad, B. Koch, S. Srikrishna, P.-Z.Li, Q. Xu and D. S. Pandey, *Inorg. Chem*., 2013, 52, 3687. (d) R. K. Gupta, G. Sharma, R. Pandey, A. Kumar, B. Koch, P.-Z. Li, Q. Xu and D. S. Pandey, *Inorg. Chem*., 2013, 52, 13984.

[6] (a) A. Alama, B. Tasso, F. Novelli and F. Sparatore, *Drug Discovery Today*, 2009, 14, 500. (b) S. Jangir, V. Bala, N. Lal, L. Kumar, A. Sarswat, L. Kumar, B. Kushwaha, P. Singh, P. K. Shukla, J. P. Maikhuri, G. Gupta and V. L. Sharma, *Org. Biomol. Chem*., 2014, 12, 3090. (c) L. Kumar, A. Sarswat, N. Lal, V. L. Sharma, A. Jain, R. Kumar, V. Verma, J. P. Maikhuri, A. Kumar, P. K. Shukla and G. Gupta, *Eur. J. Med. Chem*., 2010, 45, 817.

[7] (a) G. Hogarth, *Mini-Reviews in Medicinal Chemistry*, 2012, 12, 1202. (b) J. C. Joyner, J. Reichfield and J. A. Cowan, *J. Am. Chem. Soc*., 2011, 133, 15613. (c) J. Lv, T. Liu, S. Cai, X. Wang, L. Liu and Y. Wang, *J. Inorg. Biochem*., 2006, 100, 1888.

[8] (a) P. D. Beer, *Acc. Chem. Res.*, 1998, 31, 71. (b) P. D. Beer and P. A. Gale, *Angew. Chem., Int. Ed*., 2001, 40, 486. (c) W. H. Wong, J. Cookson, E. A. L. Evans, E. J. L. McInnes, J. Wolowska, J. P. Maher, P. Bishop and P. D. Beer, *Chem. Commun*., 2005, 2214. (d) O. D. Fox, J. Cookson, E. J. S. Wilkinson, M. G. B. Drew, E. J. MacLean, S. J. Teat and P. D. Beer, *J. Am. Chem. Soc*., 2006, 128, 6990.

[9] (a) J. L. C. Rowsell and O. M. Yaghi, *Angew. Chem., Int. Ed*. 2005, 44, 4670-4679. (b) S. J. Lippard, *Pure Appl. Chem*., 1987, 59, 731.

[10] (a) V. K. Singh, R. Kadu and H. Roy, *Eur. J. Med. Chem*., 2014, *74*, 552. (b) R. Kadu, H. Roy, V. K. Singh, *Appl. Organomet. Chem.*, 2015, 29, 746. (c) V. K. Singh, R. Kadu, H. Roy, P. Raghavaiah and S. M. Mobin, *Dalton Trans.*, 2015, 45, 1443. (d) V. Pillai, R. Kadu, L. Buch and V. K. Singh, *ChemistrySelect*, 2017, 2, 4382.

[11] T. Masui, H. Tsuda, K. Inoue, T. Ogiso and N. Ito, *Jpn. J Cancer Res.*, 1986, 77, 231.

[12] P. Tortoreto, M. Catalani, C. Bianchi, C. Blond and C. Pantarotto, *J. Chromat.*,1983, 262, 367.

[13] K. Tanaka, T. Ino, T. Sawahata, S. Marui, H. Igaki and H. Yashima, *Mutat. Res.*, 1985, 143, 11.

[14] T. Kimura, J. Hosokawa-Muto, Y. O. Kamatari and K. Kuwata, *Bioorg. Med. Chem. Lett*., 2011, 21 1502.

[15] (a) K. S. Siddiqi, S. A. A. Nami, Lutfullah and Y. Chebude, *J. Braz. Chem. Soc*., 2006, 17, 107. (b) F. Bensebaa, Y. Zhou, A. G. Brolo, D. E. Irish, Y. Deslandes, E. Kruus and T. H. Ellis, *Spectrochim. Acta*, 1999, 55A, 1229. (c) A. Z. E.-Sonbati, *Synth. React. Inorg. Met.-Org. Chem*., 1991, 21, 203.

[16] (a) G. Ercolani, *J. Phys. Chem. B*., 2003, 107**,** 5052. (b) S. Leininger, B. Olenyuk and P. J. Stang, *Chem. Rev*., 2000, 100, 853. (c) C. J. Jones, *Chem. Soc. Rev*., 1998, 27, 289.

[17] N. Yoshida and K. Ichikawa, *Chem. Commun.*, 1997, 1091.

[18] M. D. Pratt and Paul D. Beer, *Tetrahedron*, 2004, 60, 11227.

[19] (a) R. Kadu, V. Pillai, V. Amrit and V. K. Singh, *RSC Adv*., 2015, 5,106688. (b) S. Buffagni, L. M. Vallarino and J. V. Quagliaxo, *Inorganic Chemistry*, 1964, 3, 480**. (c)** A. B. P. Lever, *Inorganic Electronic Spectroscopy, Elsevier,* Amsterdam, 1984.

[20] C. R. Cardoso, M. V. S. Lima, J. Cheleski, E. J. Peterson, T. Venancio, N. P. Farrell and R. M. Carlos, *J. Med. Chem*., 2014, 57, 4906.

[21] Y. Yan, S. Krishnakumar, H. Yu, S.Ramishetti, Lih-Wen Deng, S. Wang, L. Huang and D. Huang, *J. Am. Chem. Soc*., 2013, 135, 5312.

[22] S. Das and P. K. Bharadwaj, *Inorg. Chem*., 2006, 45, 5257.

[23] V. Kumar, V. Singh, A. N. Gupta, K. K. Manar, L. B. Prasad, M. G. B. Drewb and N. Singh, *New J. Chem.*, 2014, 38, 4478.

[24] (a) H. H. Wasserman, R. W. Murray. Singlet oxygen. New York: Academic Press, 1979. (b) M. A. Caine, R. W. McCabe, L. Wang, R. G. Brown and J. D. Hepworth, *Dyes and Pigments*, 2002, 52, 55.

[25] S. Sreedaran, K. S. Bharathi, A. K. Rahiman, L. Jagadish, V. Kaviyarasan and V. Narayanan, *Polyhedron*, 2008, 27, 2931.

[26] (a) Y. Mizobe, T. Hinoue, A. Yamamoto, I. Hisaki, M. Miyata,Y. Hasegawa and N. Tohnai, *Chem. Eur. J*., 2009, 15, 8175 and the references cited in. (b) K.-H. Lee, C.-S. Choi, K.-S. Jeon, *J. Photosci*., 2002, 9, 71. (c) S. C. Martens, U. Zschieschang, H. Wadepohl, H. Klauk and L. H. Gade, *Chem. Eur. J*., 2012, 18, 3498.

[27] (a) B. F. Ali, W. S. Al- Akramawi, K. H. Al- Obaidi and A. H. A. Al-Karboli, *ThermochimicaActa*, 2004, 419, 39. (b) Sanjay K. Verma and Vinay K. Singh, *RSC Adv*., 2015, 5, 53036–53046. (c) Sanjay K. Verma and Vinay K. Singh, *J. Coord. Chem.*, 2015, 68, 1072–1087. (d) S. K. Verma and V. K. Singh, *J. Organomet. Chem*. 2015, 791, 214-224.

[28] M. J. Frisch, G. W. Trucks, H. B. Schlegel, G. E. Scuseria, M. A. Robb, J. R. Cheeseman, J. A. Montgomery Jr., T. Vreven, K. N. Kudin, J. C. Burant, J. M. Millam, S. S. Iyengar, J. Tomasi, V. Barone, B. Mennucci, M. Cossi, G. Scalmani, N. Rega, G.A. Petersson, H. Nakatsuji, M. Hada, M. Ehara, K. Toyota, R. Fukuda, J. Hasegawa, M. Ishida, T. Nakajima, Y. Honda, O. Kitao, H. Nakai, M. Klene, X. Li, J. E. Knox, H. P. Hratchian, J. B. Cross, C. Adamo, J. Jaramillo, R. Gomperts, R. E. Stratmann, O. Yazyev, A. J. Austin, R. Cammi, C. Pomelli, J. W. Ochterski, P. Y. Ayala, K. Morokuma, G. A. Voth, P. Salvador, J. J. Dannenberg, V. G. Zakrzewski, S. Dapprich, A. D. Daniels, M. C. Strain, O. Farkas, D. K. Malick, A. D. Rabuck, K. Raghavachari, J.

B. Foresman, J. V. Ortiz, Q. Cui, A. G. Baboul, S. Clifford, J. Cioslowski, B. B. Stefanov, G. Liu, A. Liashenko, P. Piskorz, I. Komaromi, R. L. Martin, D. J. Fox, T. Keith, M. A. A.-Laham, C. Y. Peng, A. Nanayakkara, M. Challacombe, P. M. W. Gill, B. Johnson, W. Chen, M. W. Wong, C. Gonzalez, J. A. Pople, Gaussian, Inc., Wallingford, CT, 2004.

[29] (a) D. Ghosh, K. Sen and A. K. Das, *Struct Chem*., 2012, 23, 227. (b) X. Yu, N. Wang, H. He and L. Wang, *SpectrochimActa A*, 2014, 122, 283. (c) M. Dolores Palacios, M. C. Puerta, P. Valerga, A. Lledos, and E. Veilly, *Inorg. Chem*., 2007, 46, 6958.

[30] (a) P. D. Beer, A. G. Cheetham, M. G. B. Drew, O. Danny Fox, J. Elizabeth Hayes and T. D. Rolls, *Dalton Trans*., 2003, *4*, 603–611.(b) J. Cookson, E. A. L. Evans, J. P. Maher, C. J. Serpell, R. L. Paul, A. R. Cowley, M. G. B. Drew, P. D. Beer, *Inorg. Chim. Acta.*, 2010, 363, 1195. (c) Siu-Wai Lai, M. G. B. Drew and P. D. Beer, *J. Organomet. Chem*., 2001, 637–639, 89–93.

[31] J. W. Swardstrom, L. A. Duvall and D. P. Miller *Acta Cryst.*, 1972, B28, 2510.

[32] M. Sundermann, V. Knasmüller, S. Wu, X. J. Darroudi and F. Kassie, *Toxicology*, 2004, 1–3, 329.

[33] G. Douglas, 2011 Means to an End: Apoptosis and other Cell Death Mechanisms. Cold Spring Harbor, NY: Cold Spring Harbor Laboratory Press. ISBN 978-0-87969-888-1.

[34] A. K.Taraphdar, M. Roy and R. Bhattacharya, *Curr. Sci.*, 2001, 80, 1387.

[35] M. P. Mattson, *Brain Pathology*, 2000, 10, 300.

[36] K. Liu, P. C. Liu, R. Liu, and X.Wu, *Med. Sci. Monit. Basic Res.*, 2015, 21, 15.

[37] (a) P. Manisankar, A. Sarpudeen and S. Viswanathan, *Biomed. Anal*., 2001, 26, 873. (b)

H. Oelschlaeger and G. Modrack, *Arch. Pharm*., 1986, 319, 10. (c) H. Yang, X. Chen, W. Jiang and Y. Lu, *Inorg. Chem. Commun*., 2005, 8, 853. (d) S. K. Verma, R. Kadu and V. K. Singh, *Nano-Met. Chem*., 2014, 44, 44.

[38] T. V. Berghe, S. Grootjans, V. Goossens, Y. Dondelinger, D. V. Krysko, N. Takahashi and P. Vandenabeele, *Methods*, 2013, 61, 117.

[39] S. Kasibhatla, G. P. A.-Mendes, D. Finucane, T. Brunner, E. Bossy-Wetzel and D. R. Green, *Cold Spring Harb. Protoc.*, 2006, 3, 4493.

3.6 Annexures:

3.6.1 Spectral characterization

Mass spectra

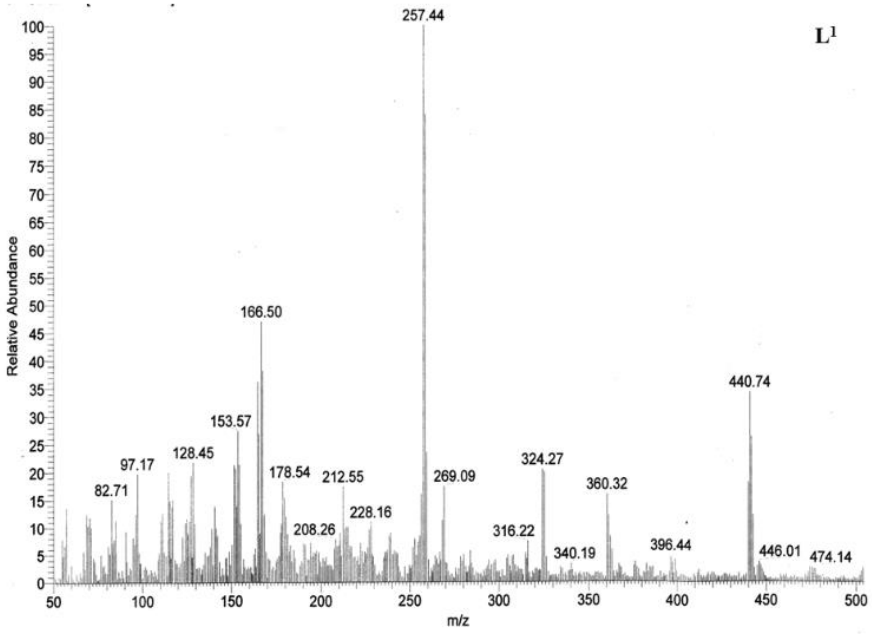

Annexure 1. Mass spectrum of L^1.

.

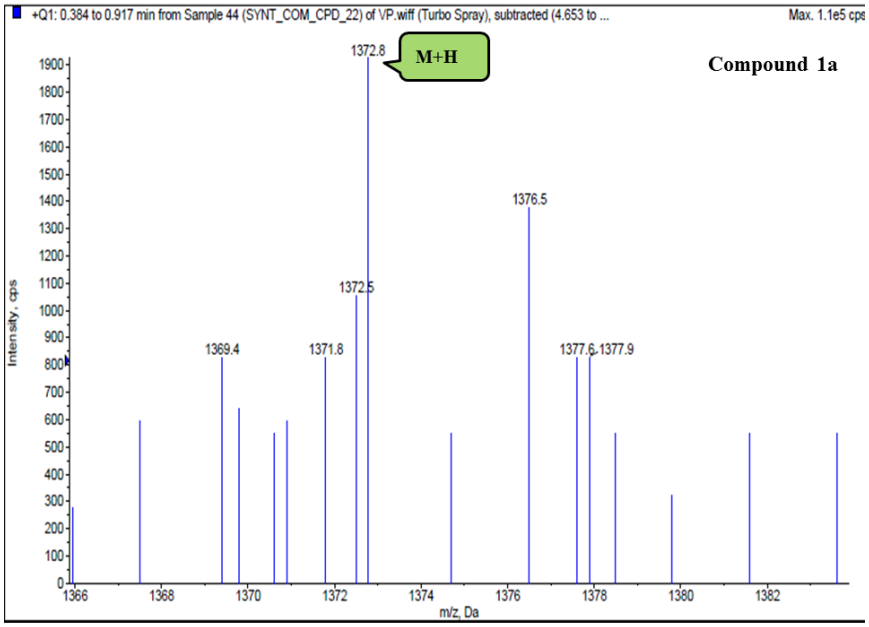

Annexure 2. Mass spectrum of 1a.

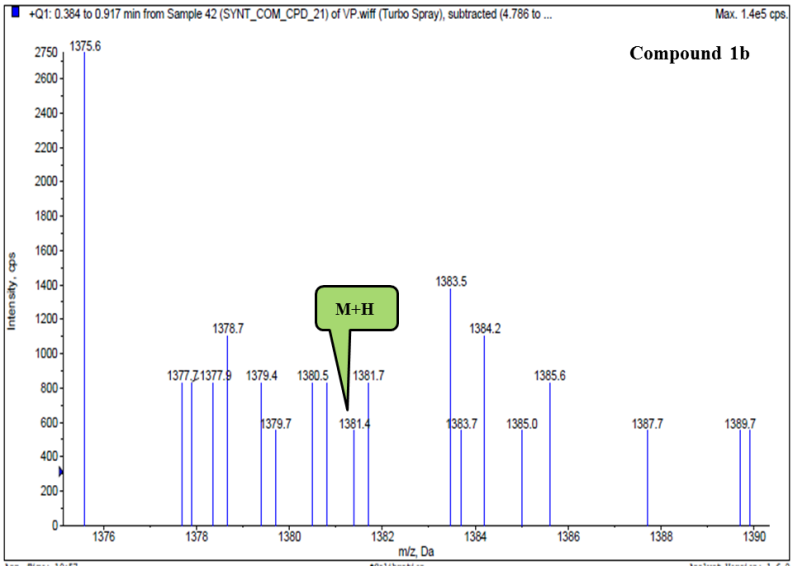

Annexure 3. Mass spectrum of 1b.

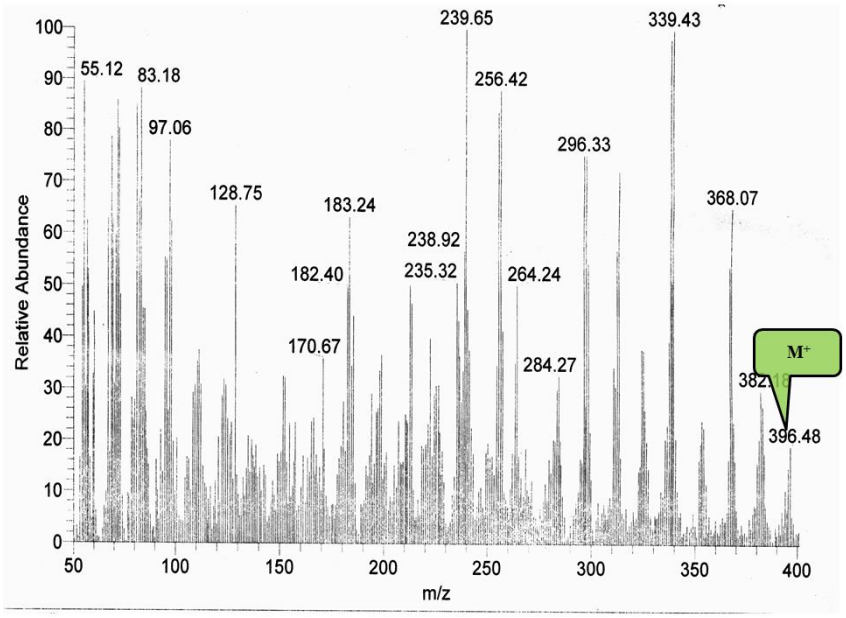

Annexure 4. Mass spectrum of L^2.

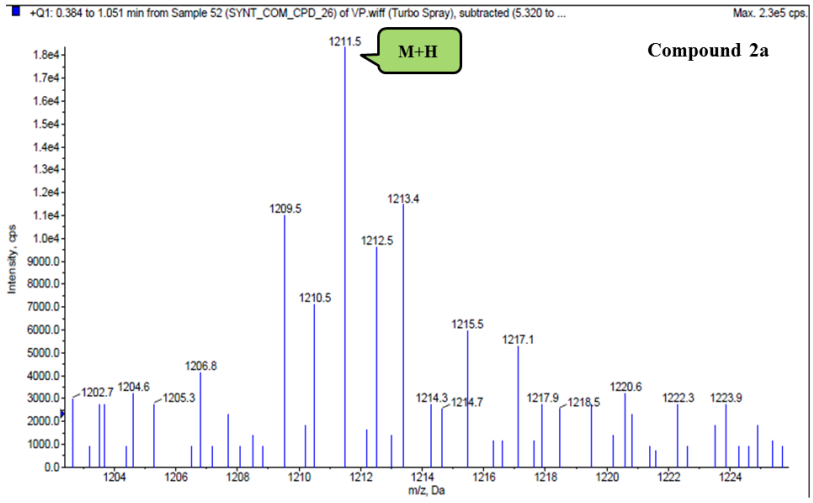

Annexure 5. Mass spectrum of 2a.

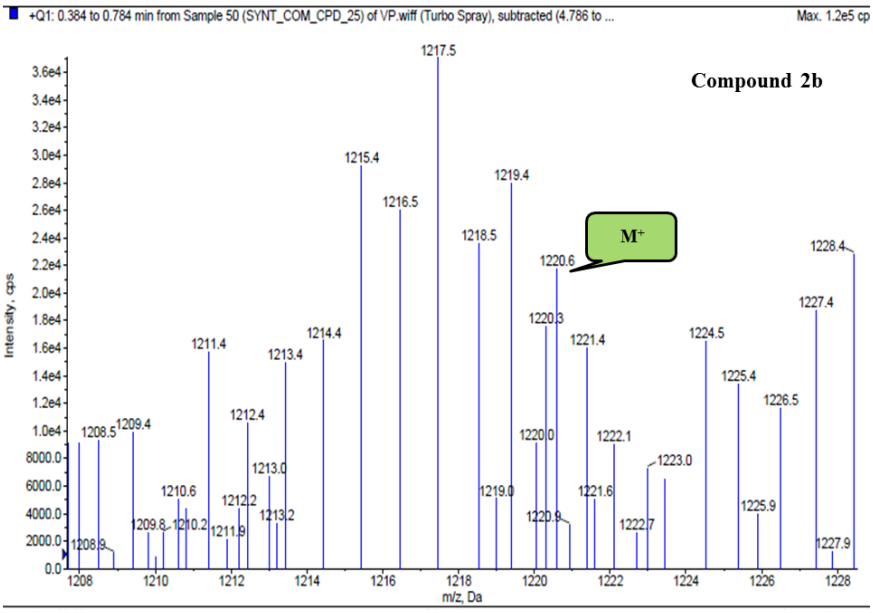

Annexure 6. Mass spectrum of 2b.

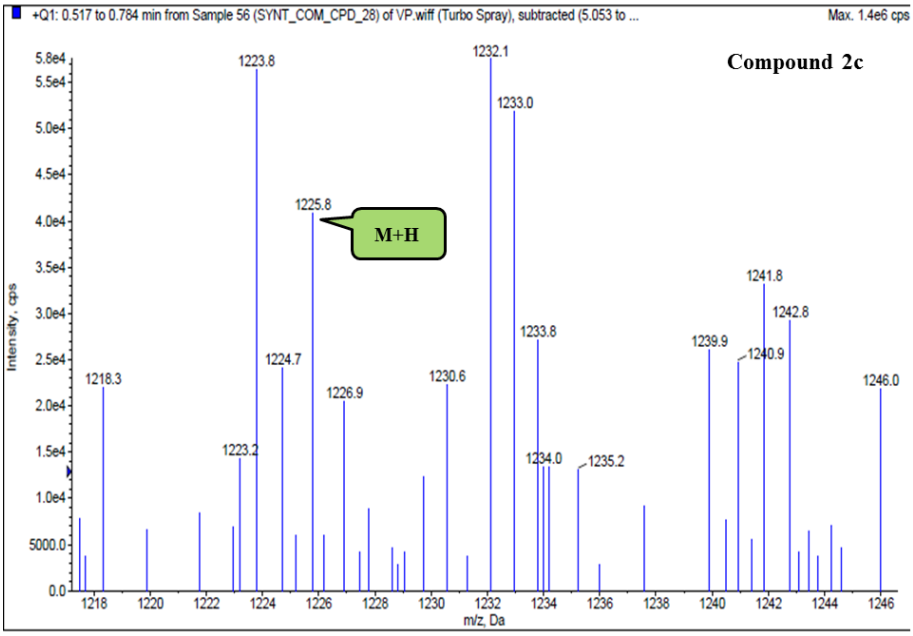

Annexure 7. Mass spectrum of 2c.

IR spectral data

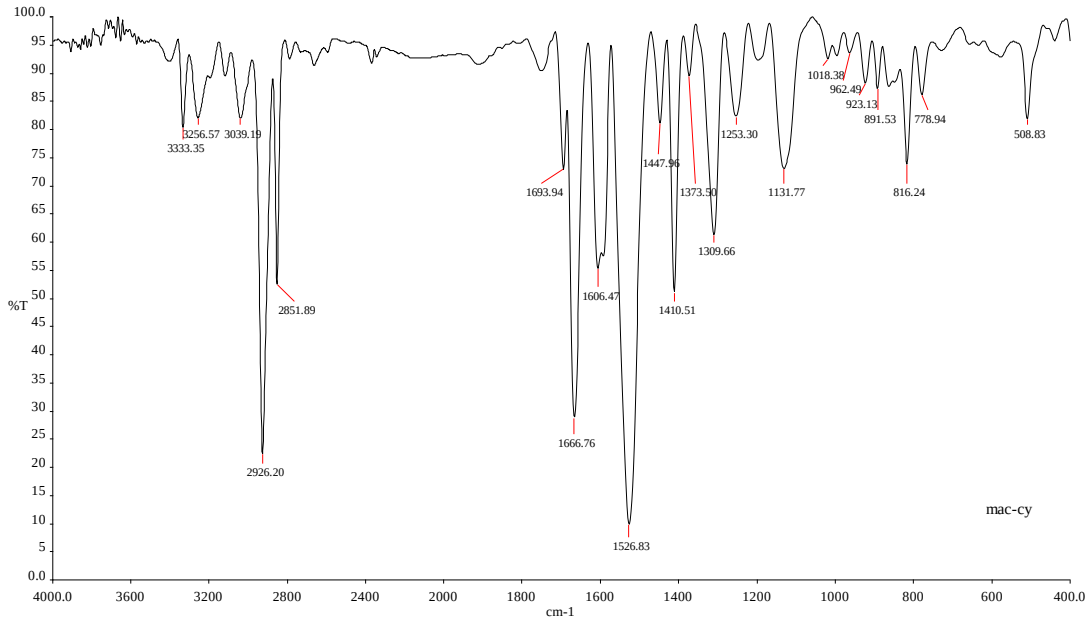

Annexure 8. IR spectrum of L^1

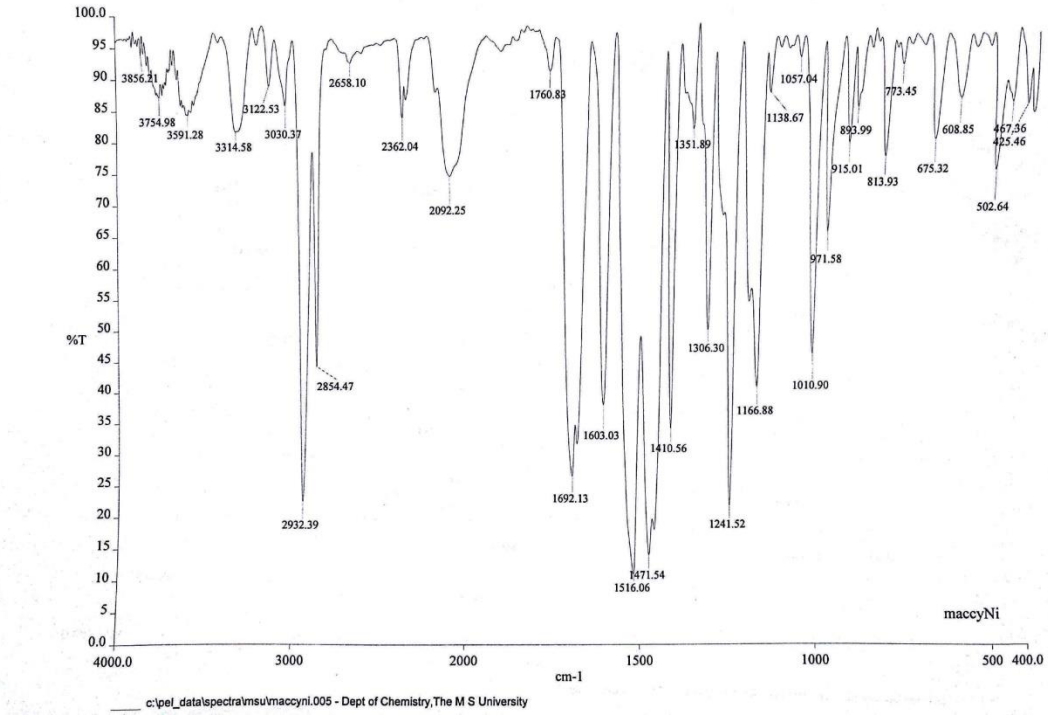

Annexure 9. IR spectrum of 1a

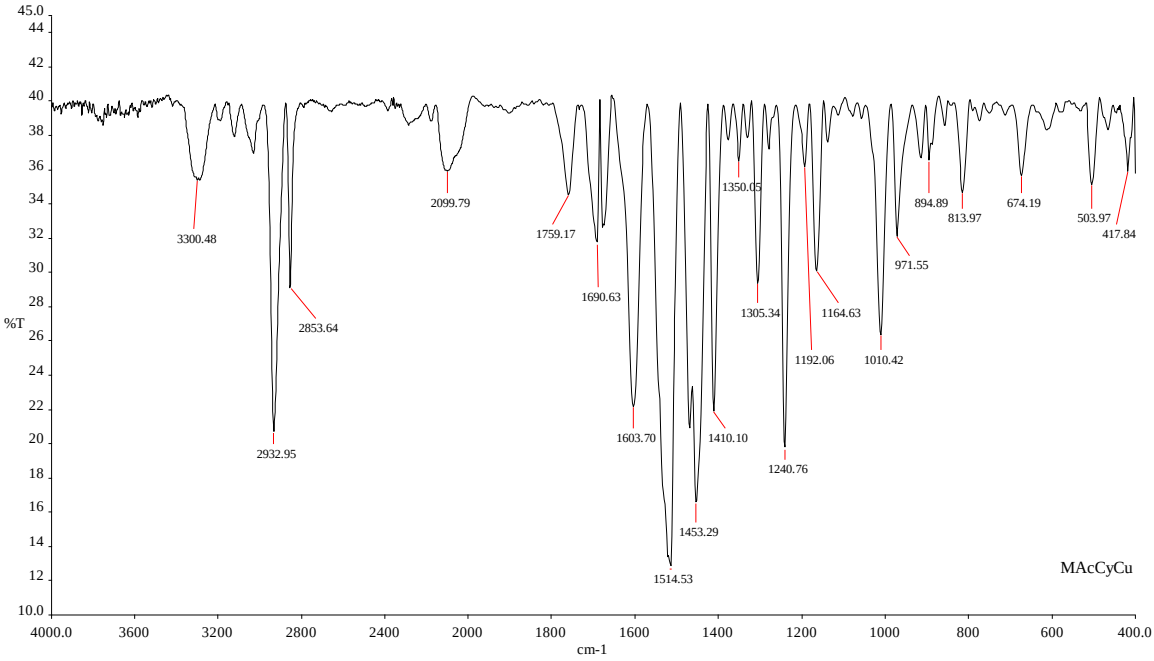

Annexure 10. IR spectrum of 1b

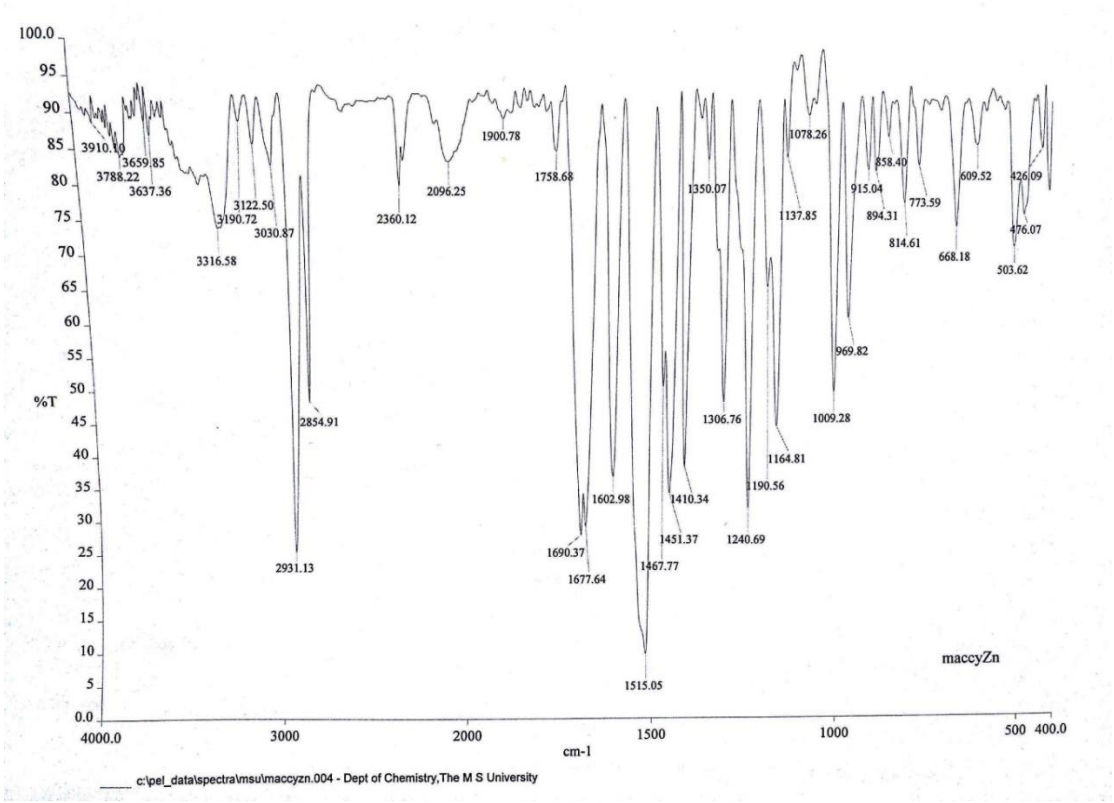

Annexure 11. IR spectrum of 1c

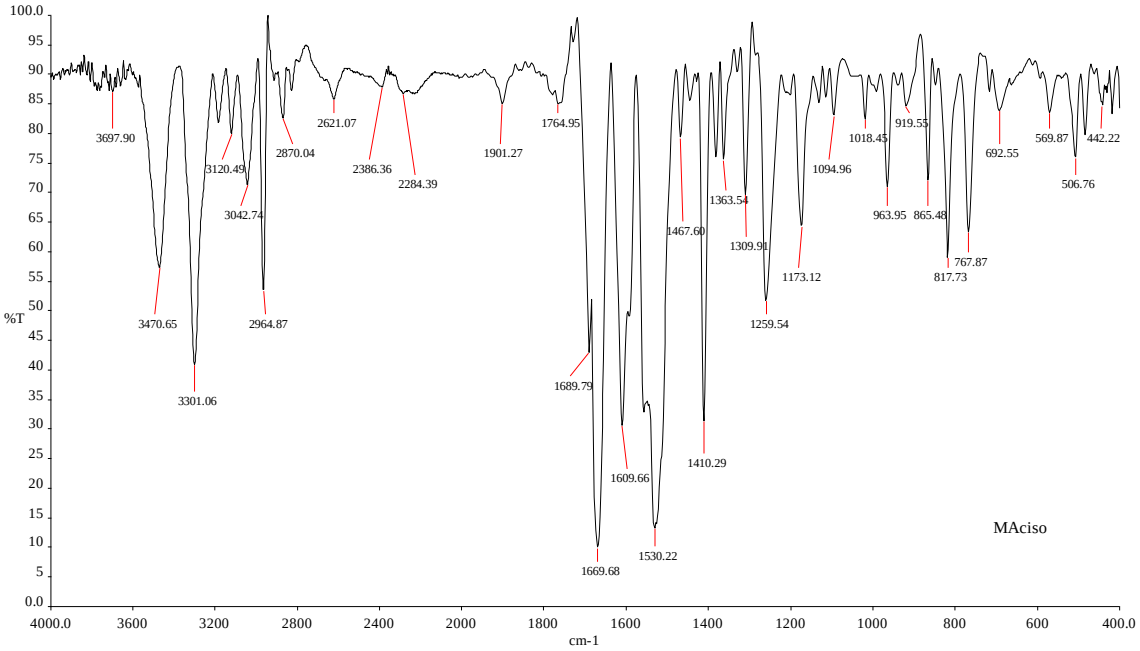

Annexure 12. IR spectrum of $\mathbf{L^2}$

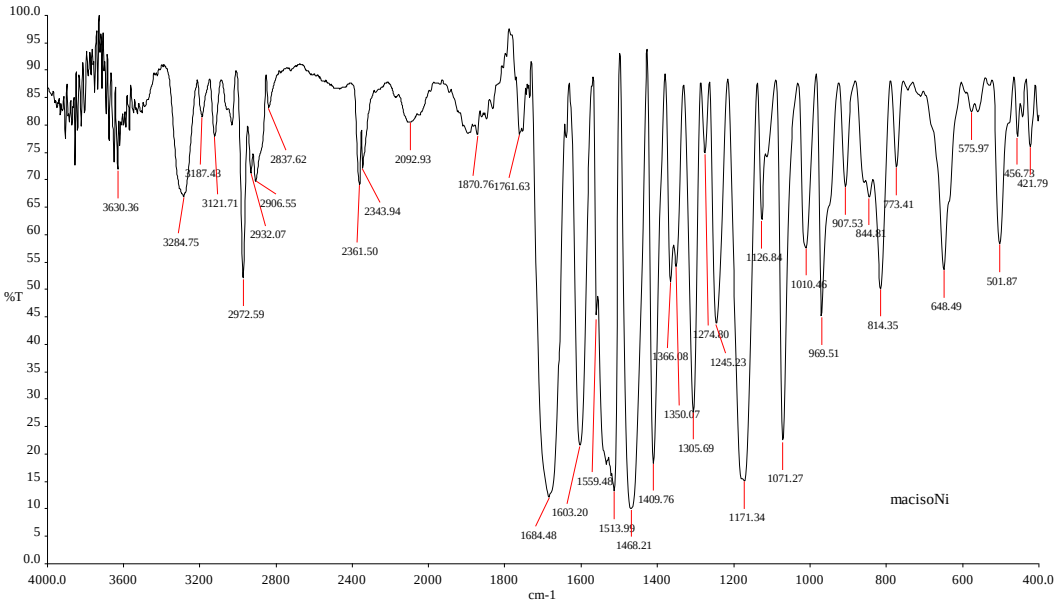

Annexure 13. IR spectrum of **2a**

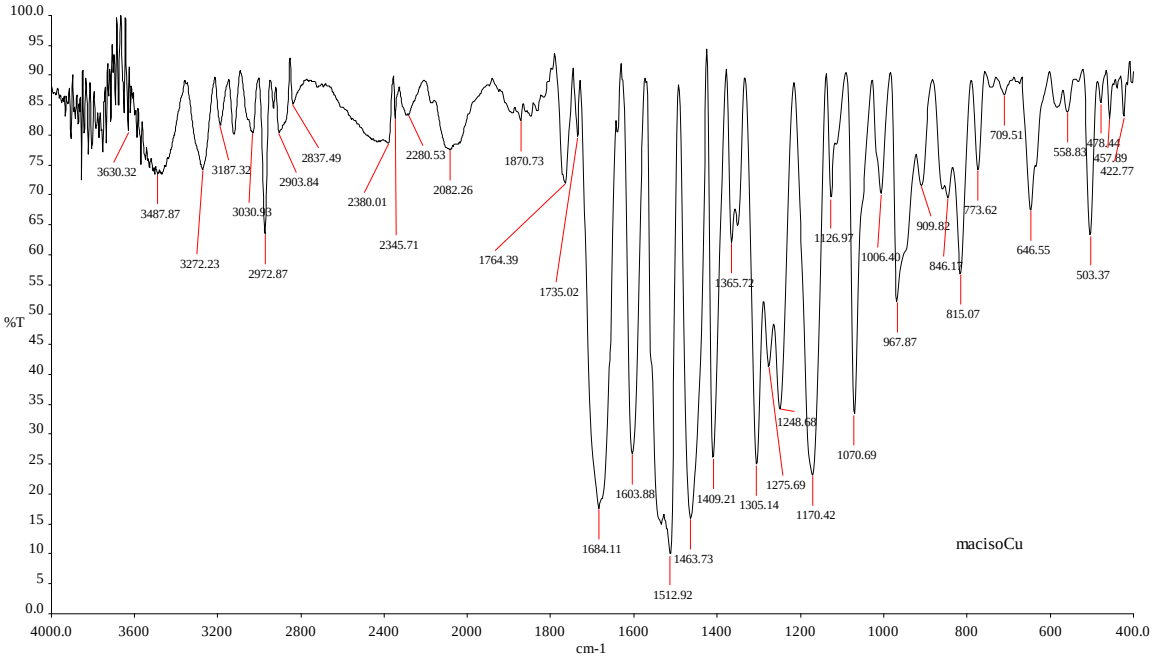

Annexure 14. IR spectrum of **2b**

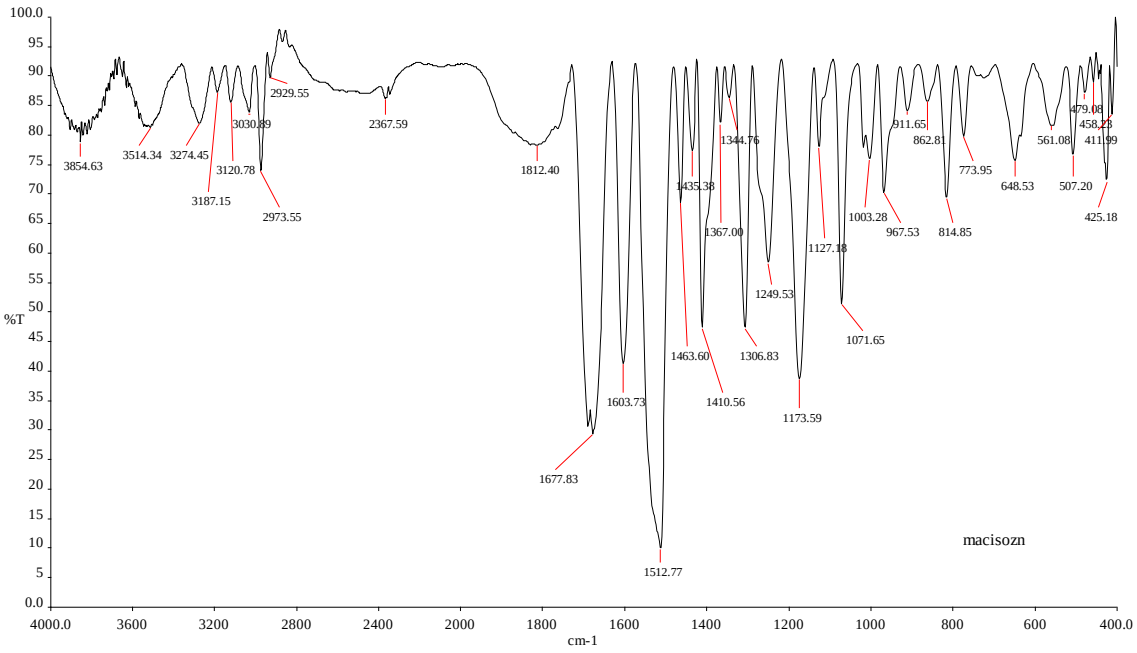

Annexure 15. IR spectrum of **2c**

NMR spectral data

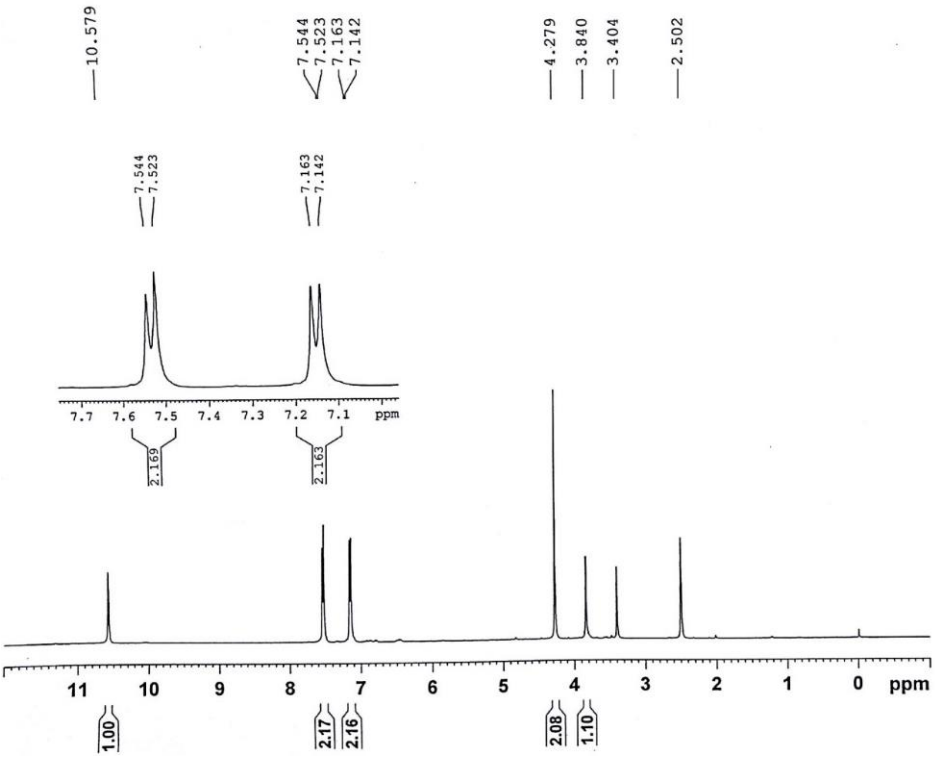

Annexure 16. ^{1}H NMR spectrum of L' inDMSO-d_6.

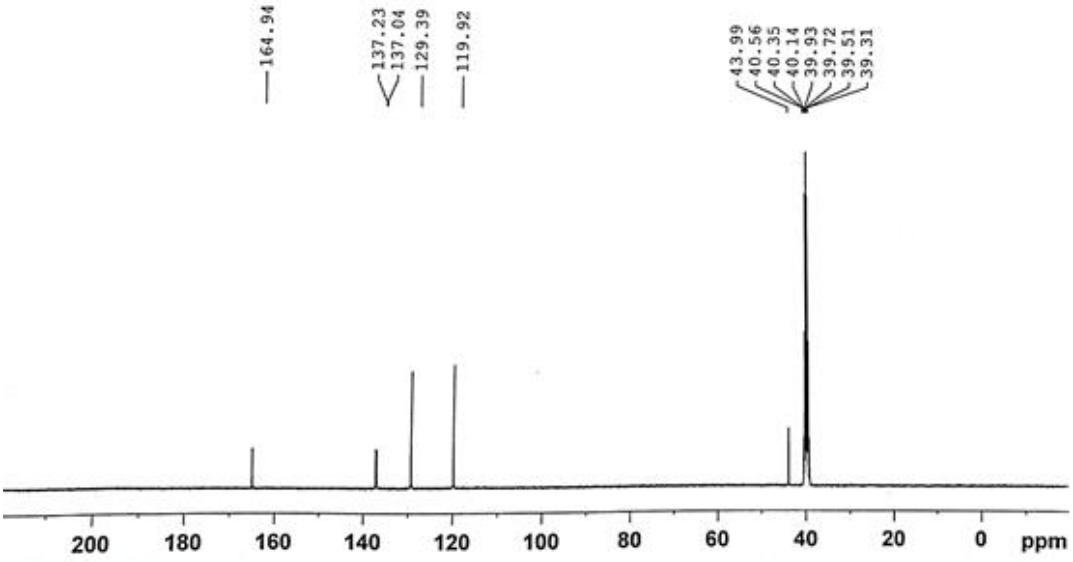

Annexure 17. ^{13}C NMR spectrum of L' inDMSO-d_6.

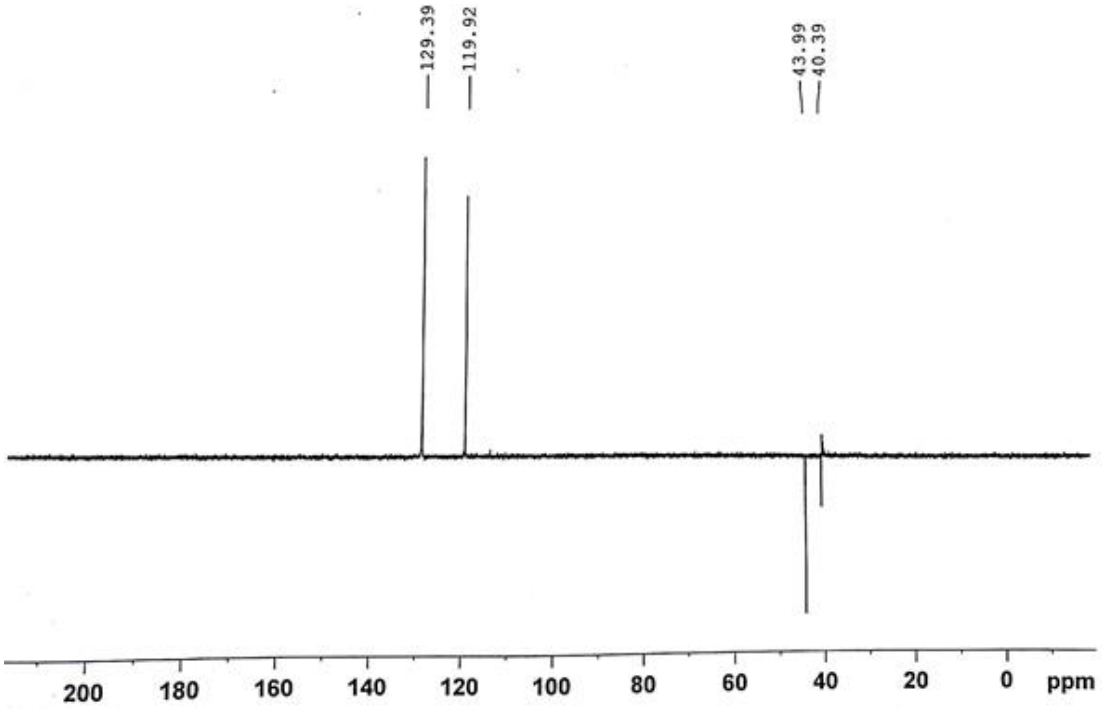

Annexure 18. DEPT-135 spectrum of L'.

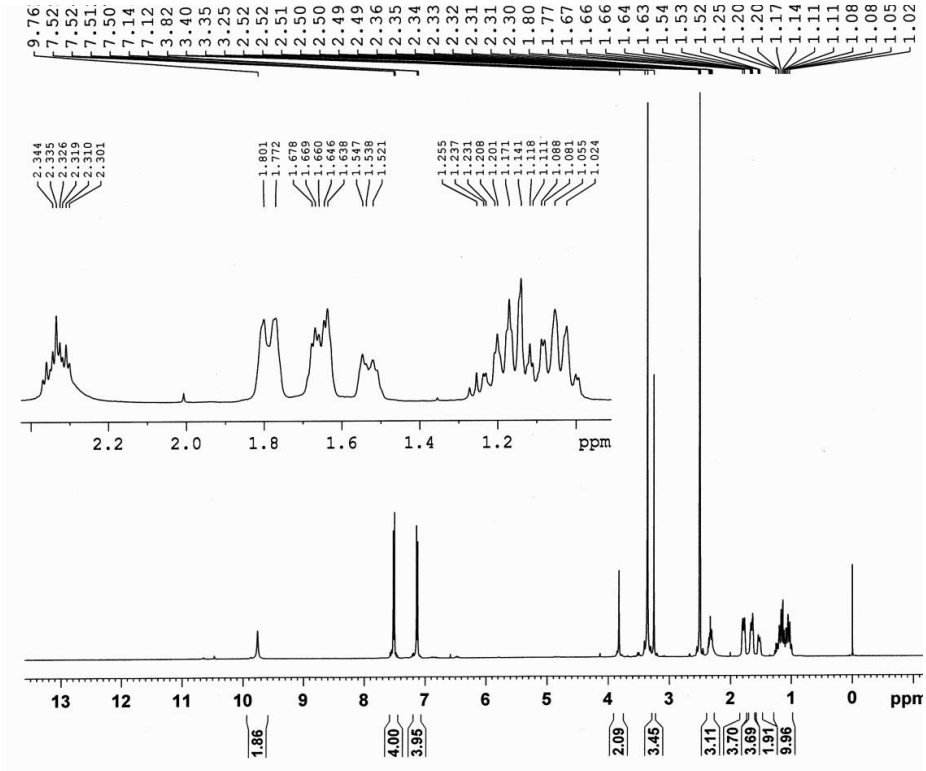

Annexure 19. ^{1}H NMR spectrum of L^{1}.

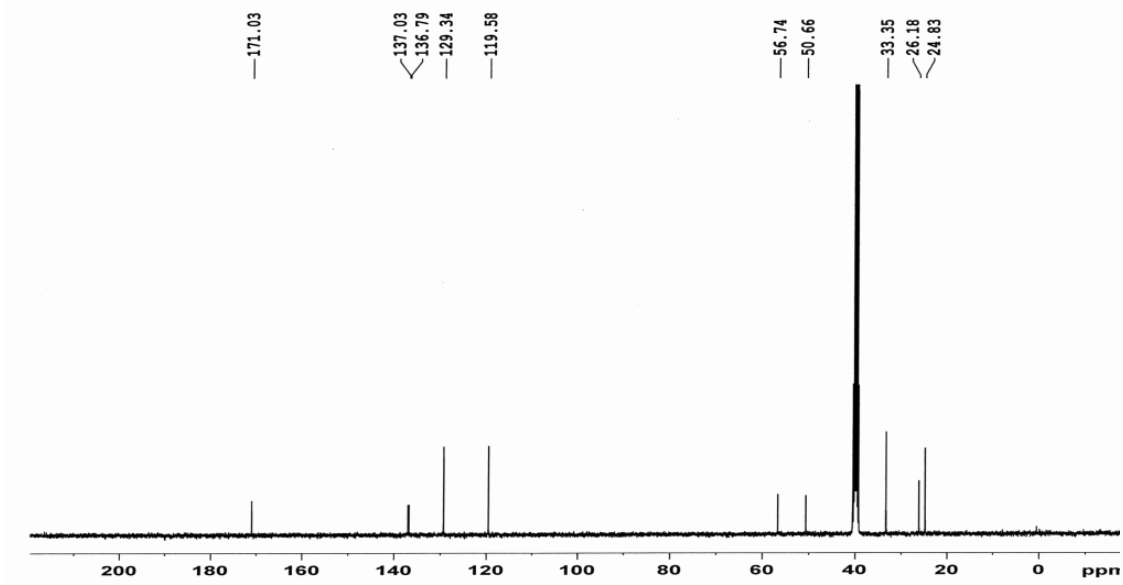

Annexure 20. ^{13}C NMR spectrum of L^1.

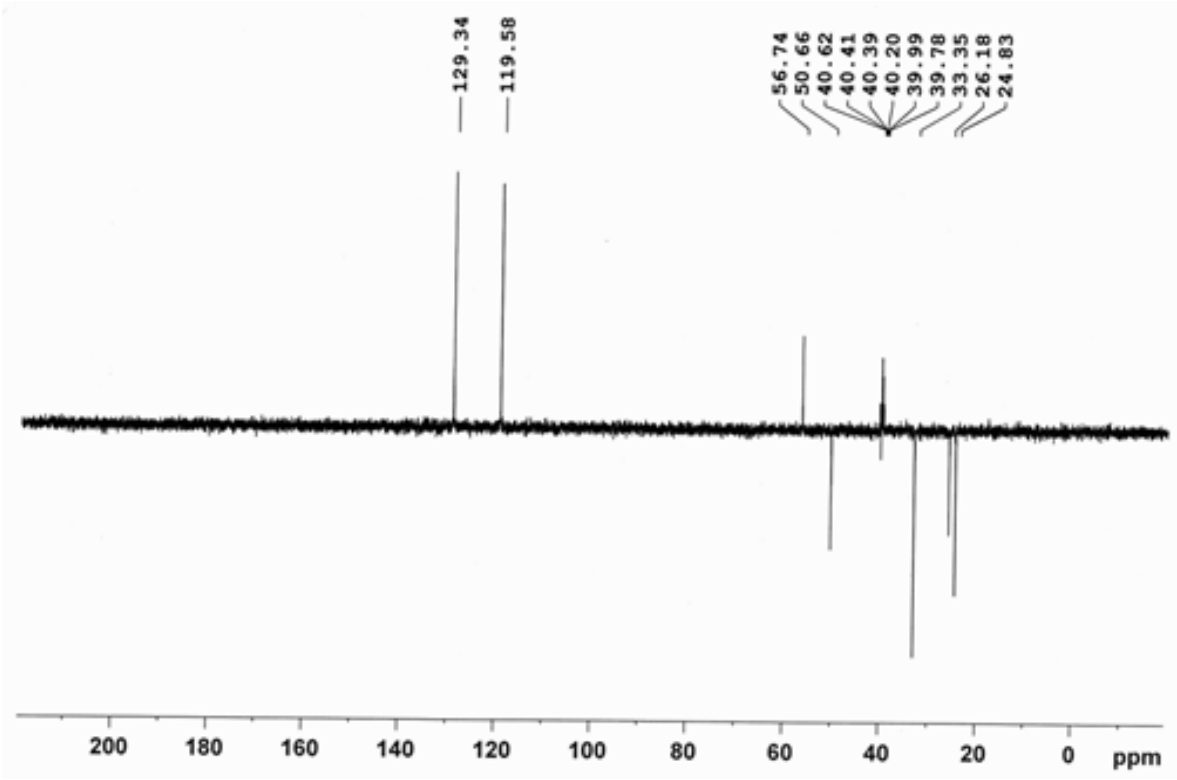

Annexure 21. DEPT-135 spectrum of L^1.

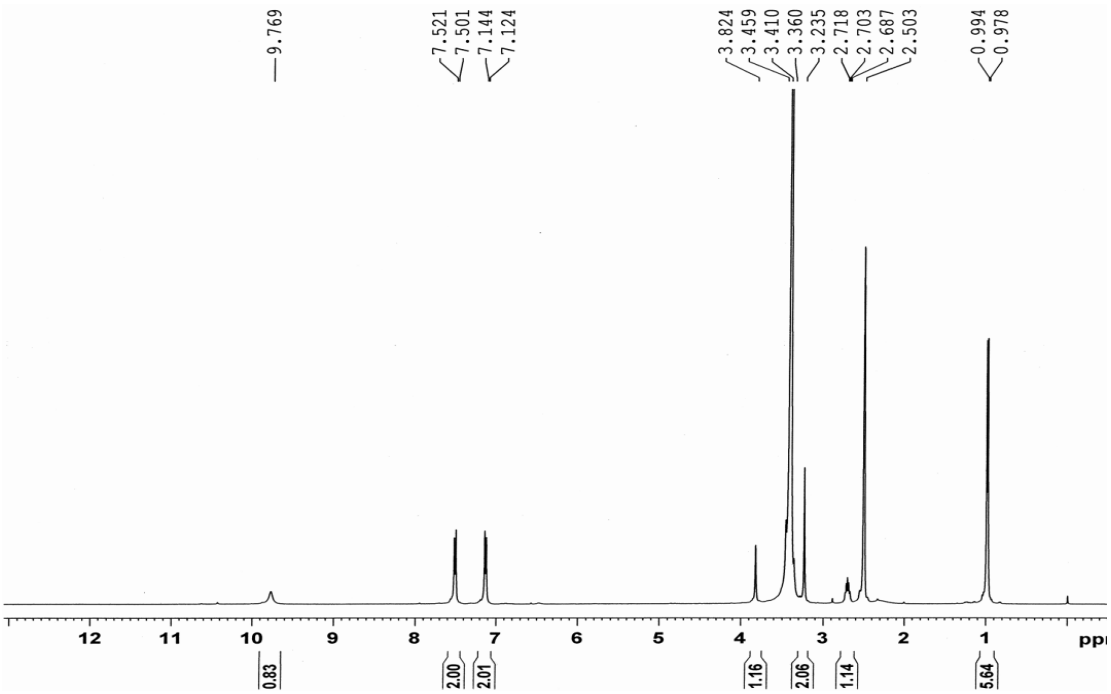

Annexure 22. ^{1}H NMR spectrum of L^{2}.

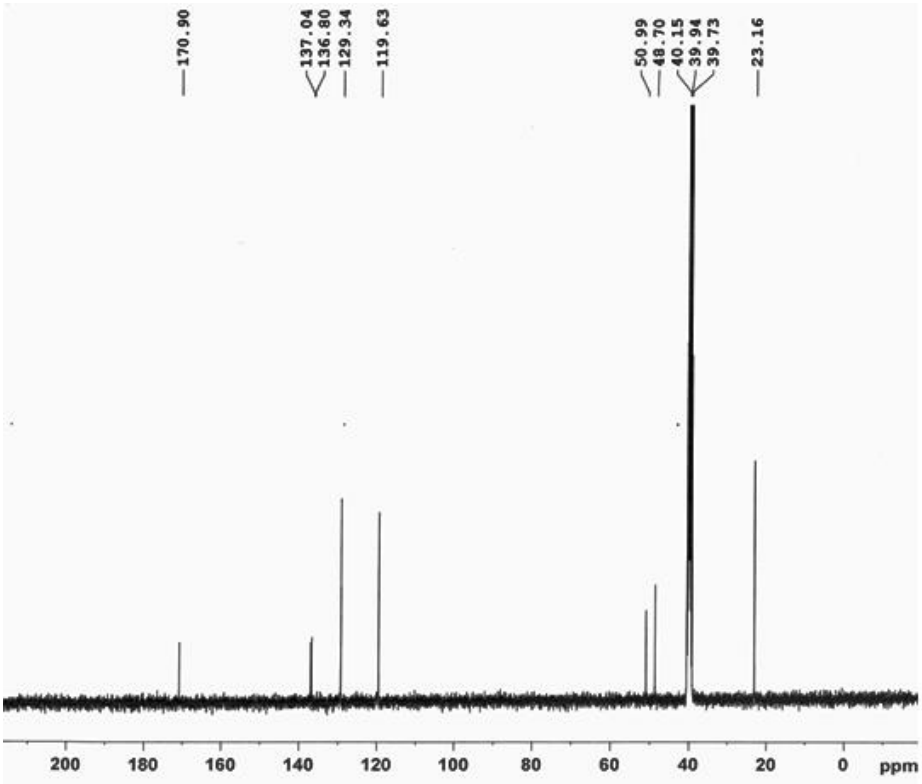

Annexure 23. ^{13}C NMR spectrum of L^{2}.

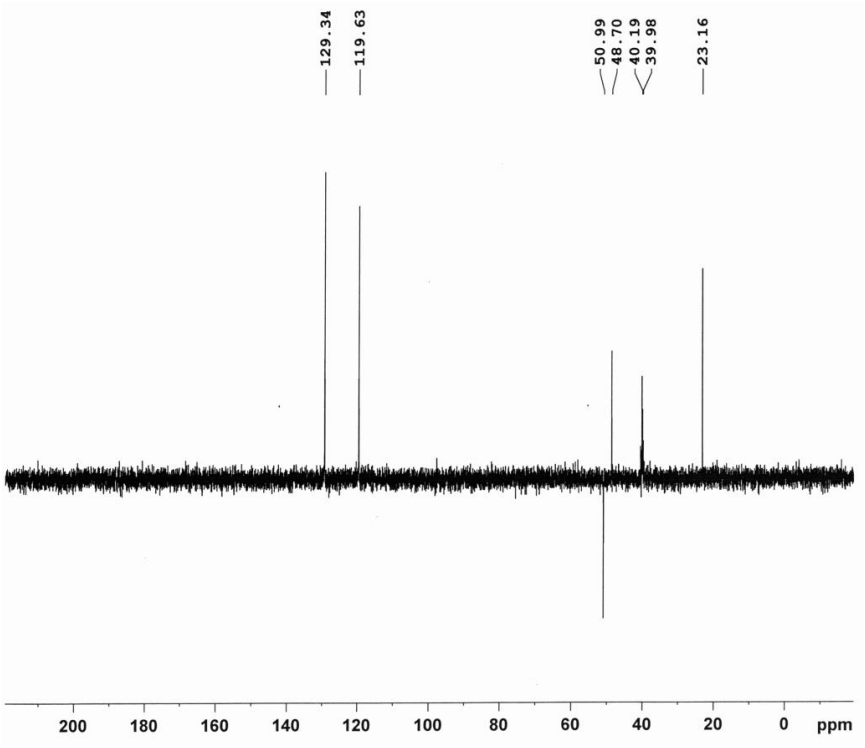

Annexure 24. DEPT-135 spectrum of L^2.

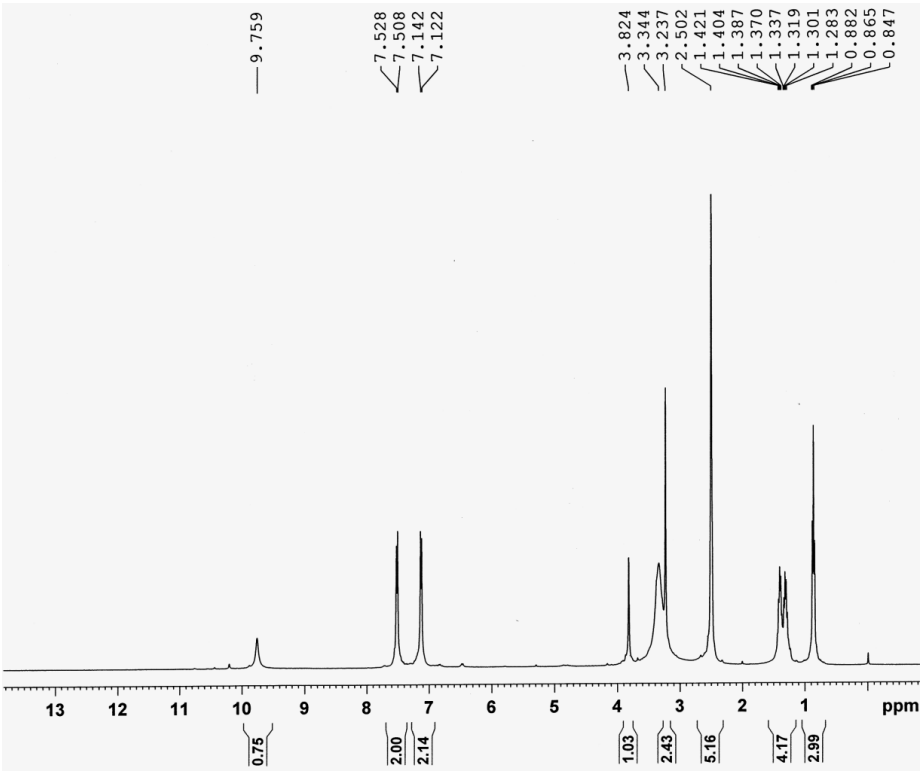

Annexure 25. ^{1}H NMR spectrum of L^3.

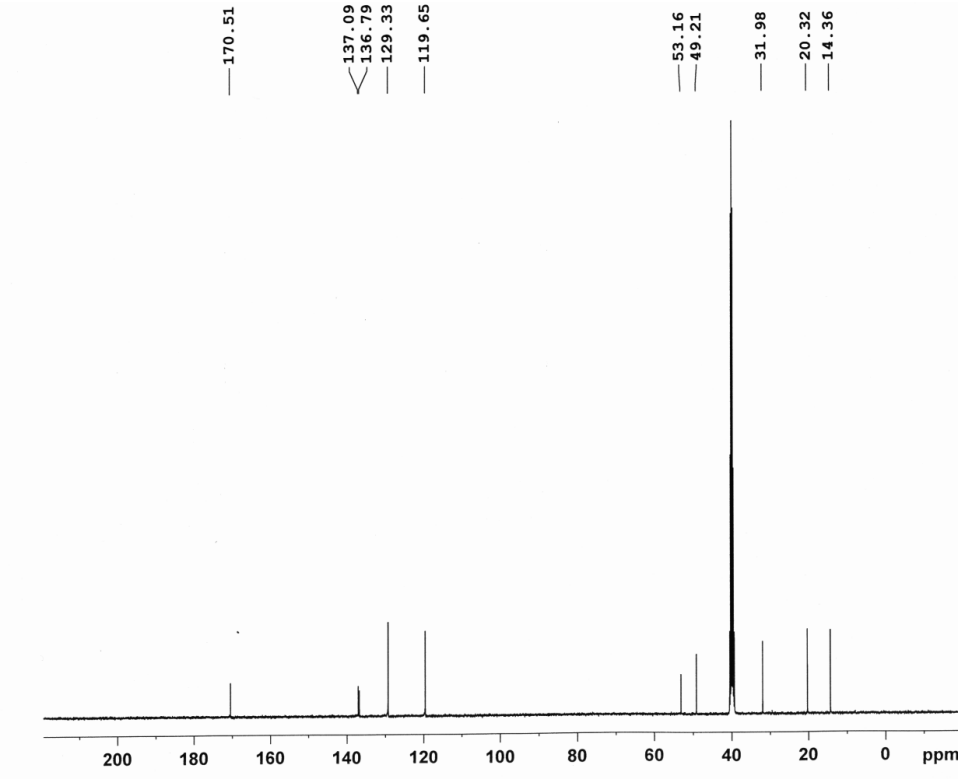

Annexure 26. ^{13}C NMR spectrum of L^3.

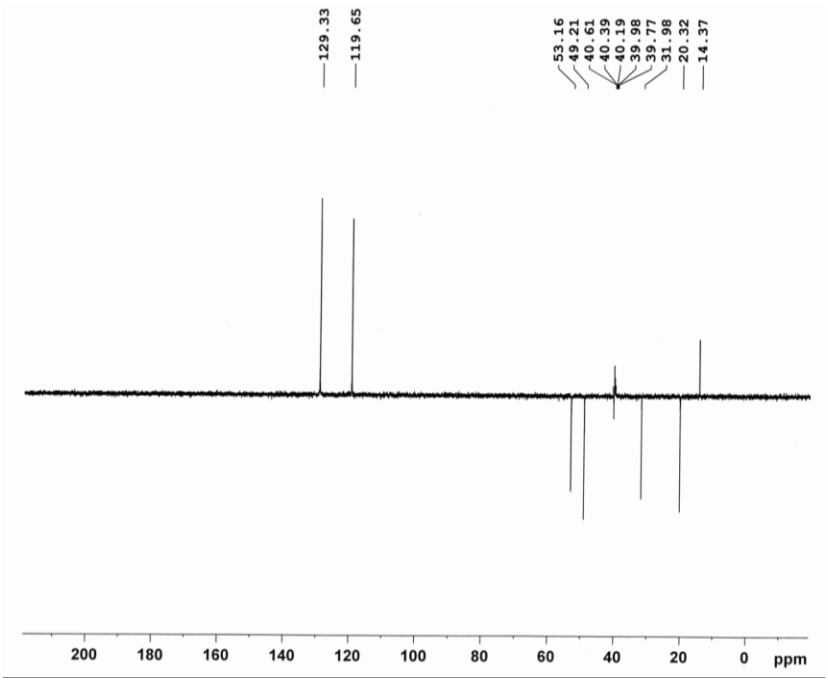

Annexure 27. DEPT-135 spectrum of L^3.

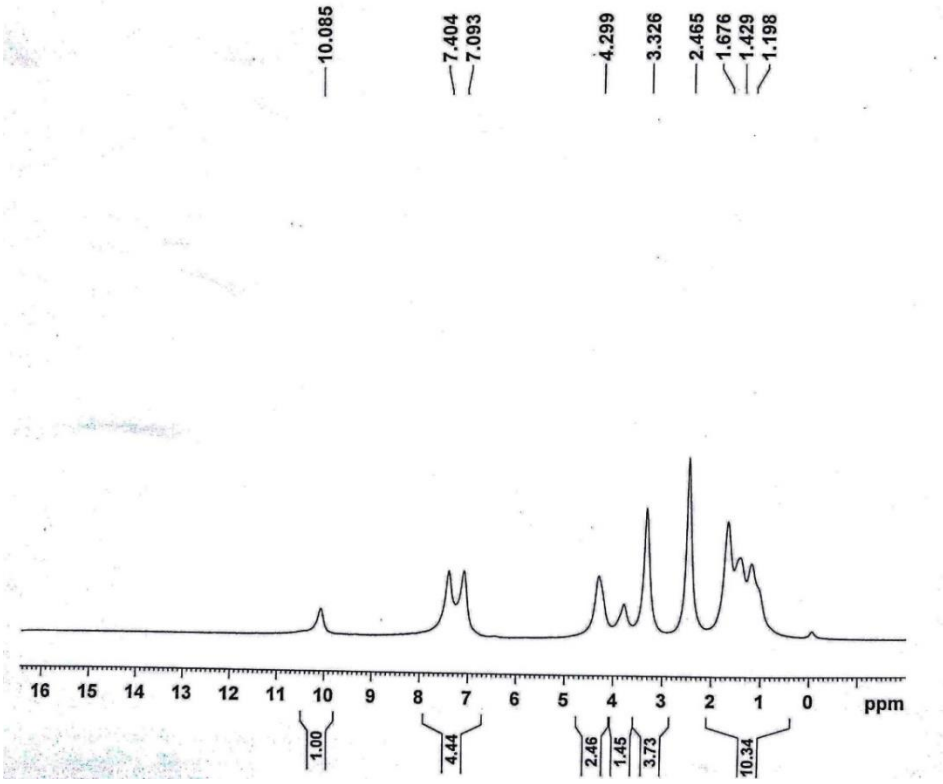

Annexure 28. ^{1}H NMR spectrum of **1a** in DMSO-d6.

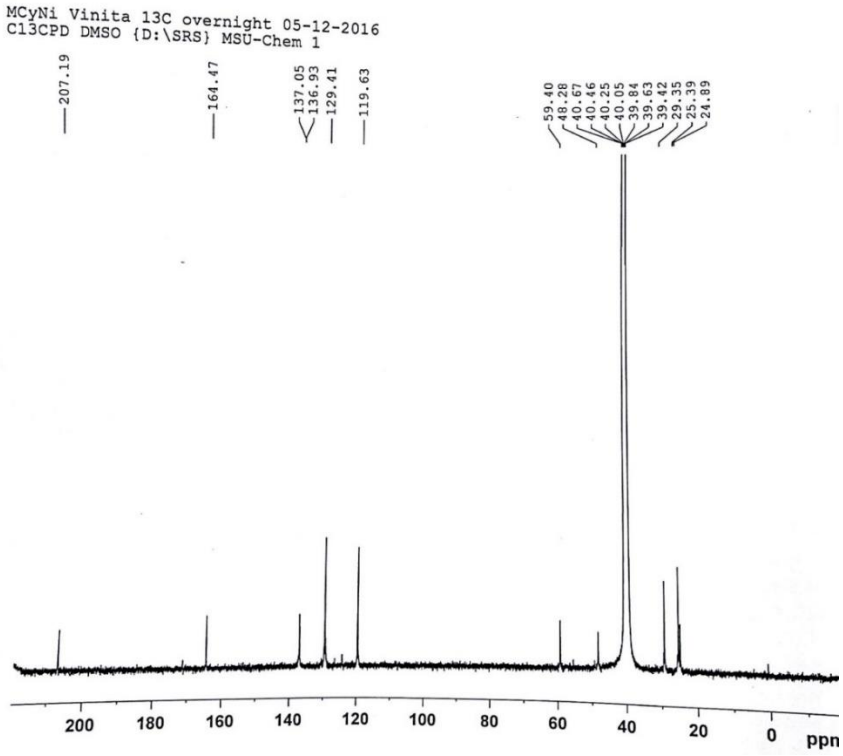

Annexure 29. ^{13}CNMR spectrum of **1a** in DMSO-d6.

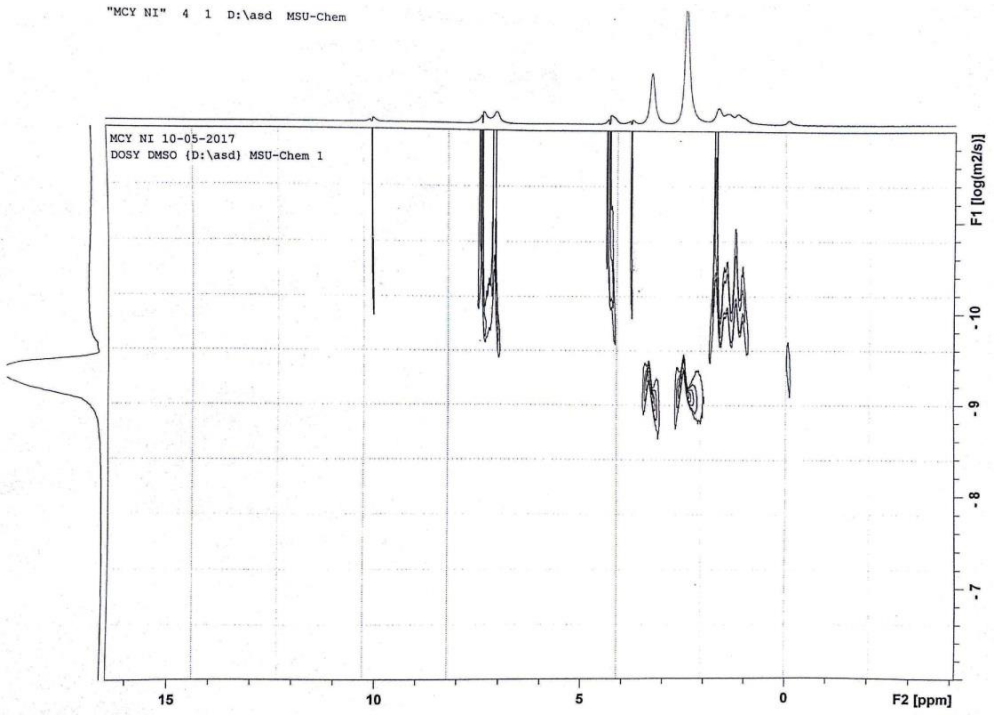

Annexure 30. DOSY NMR spectrum of 1a.

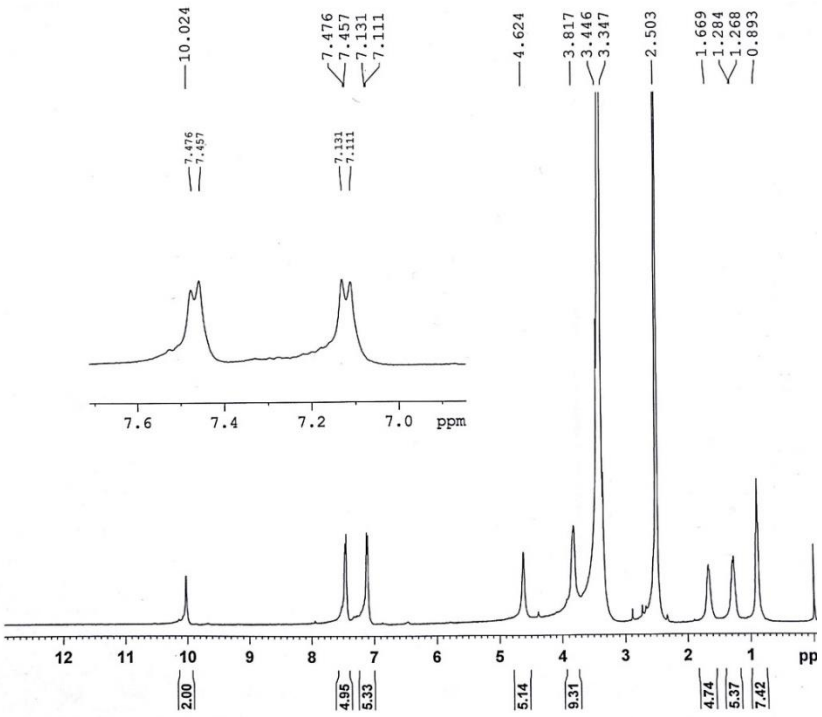

Annexure 31. ^{1}H NMR spectrum of 1c in DMSO-d6.

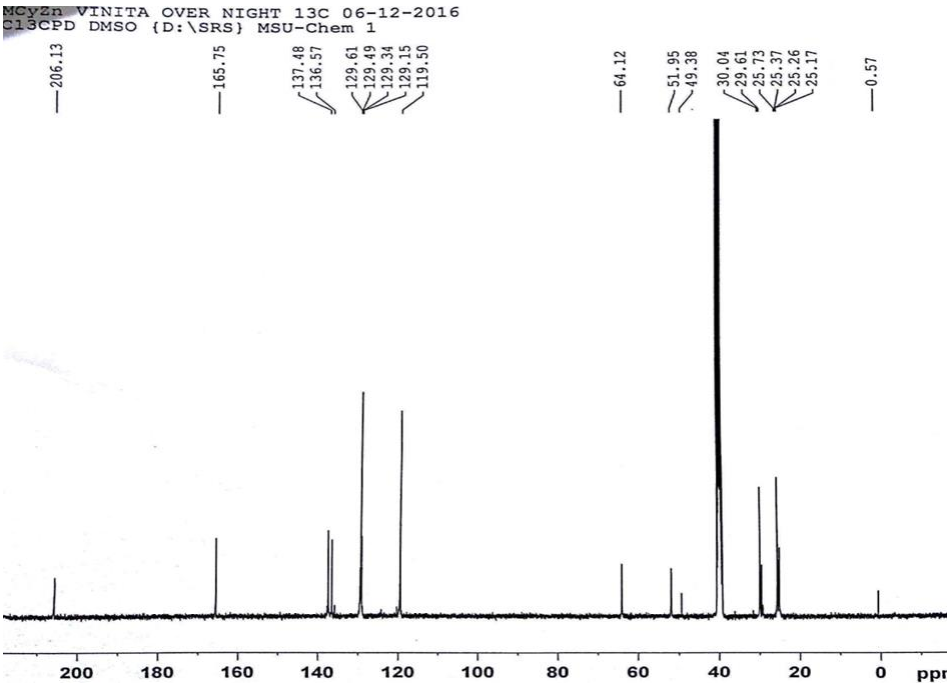

Annexure 32. ^{13}C NMR spectrum of 1c in DMSO-d6.

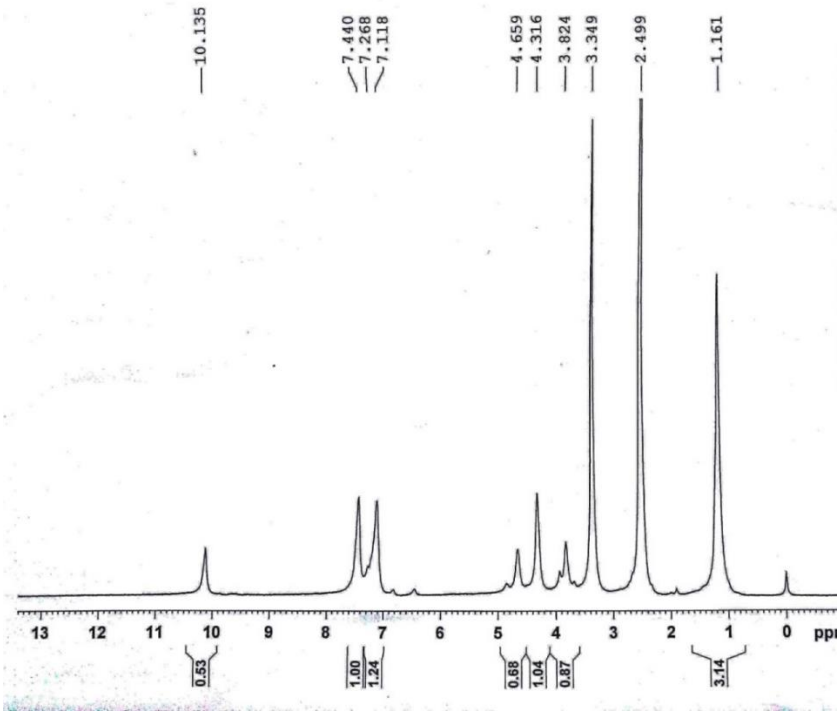

Annexure 33. ^{1}H NMR spectrum of 2**a** in DMSO-d6

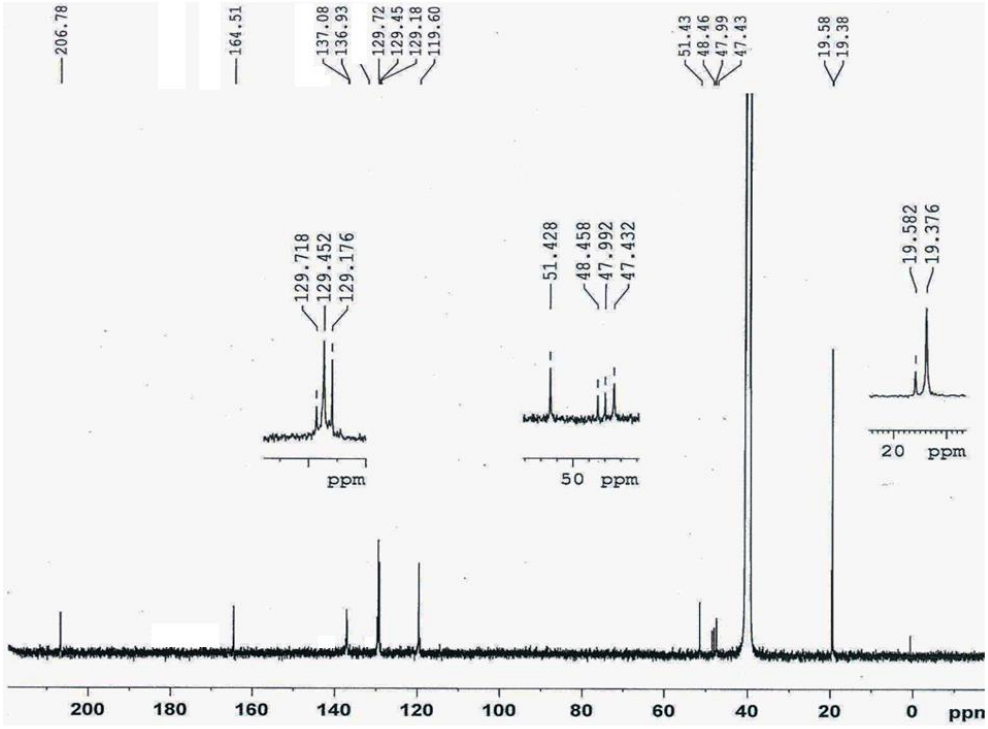

Annexure 34. ^{13}C NMR spectrum of 2**a** in DMSO-d6

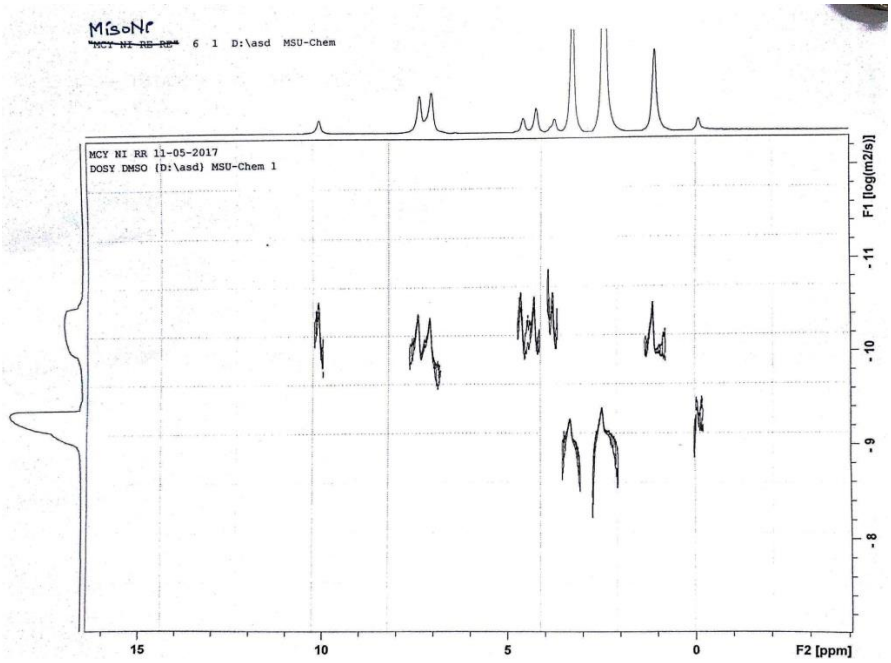

Annexure 35. DOSY NMR spectrum of 2a.

.

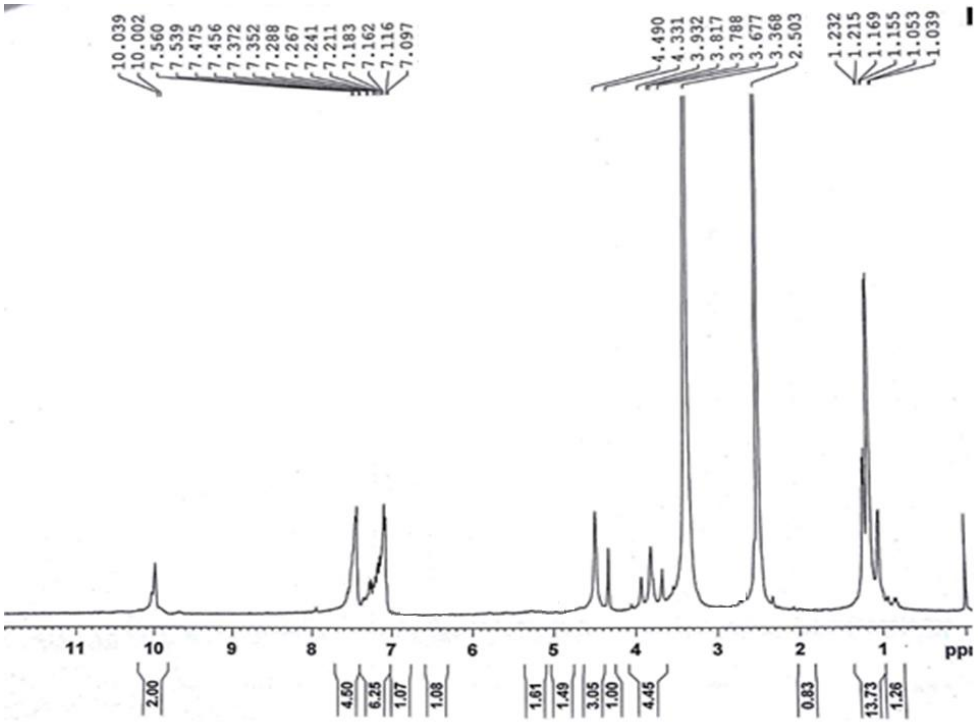

Annexure 36. ^{1}H NMR spectrum of 2c in DMSO-d6

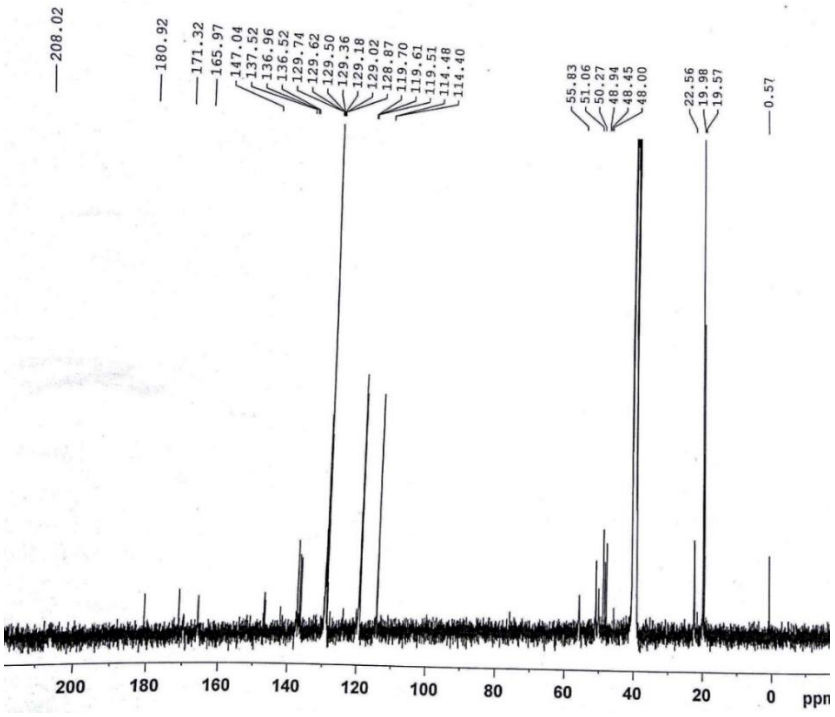

Annexure 37. ^{13}C NMR spectrum of 2c in DMSO-d6

UV-visible absorption spectra:

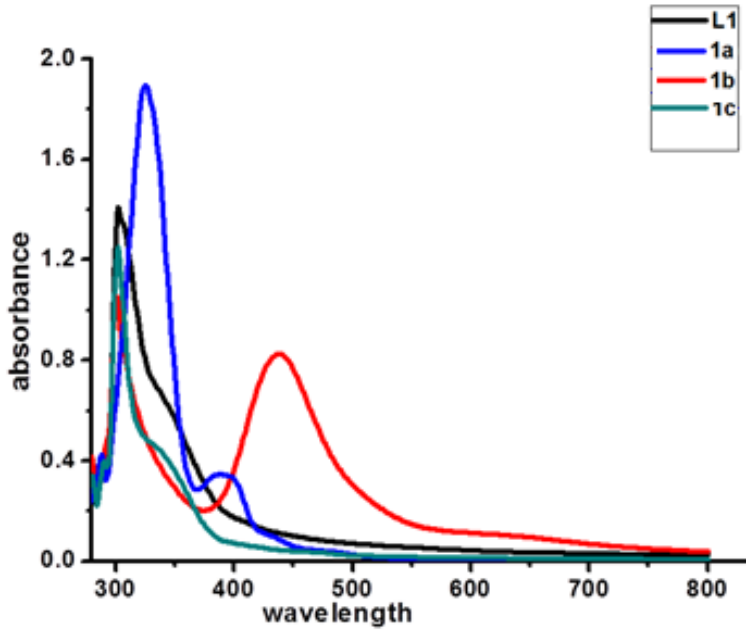

Annexure 38. UV–visible absorption spectra of compounds $\mathbf{L^1}$ and **1a, 1b, 1c** in DMF solution.

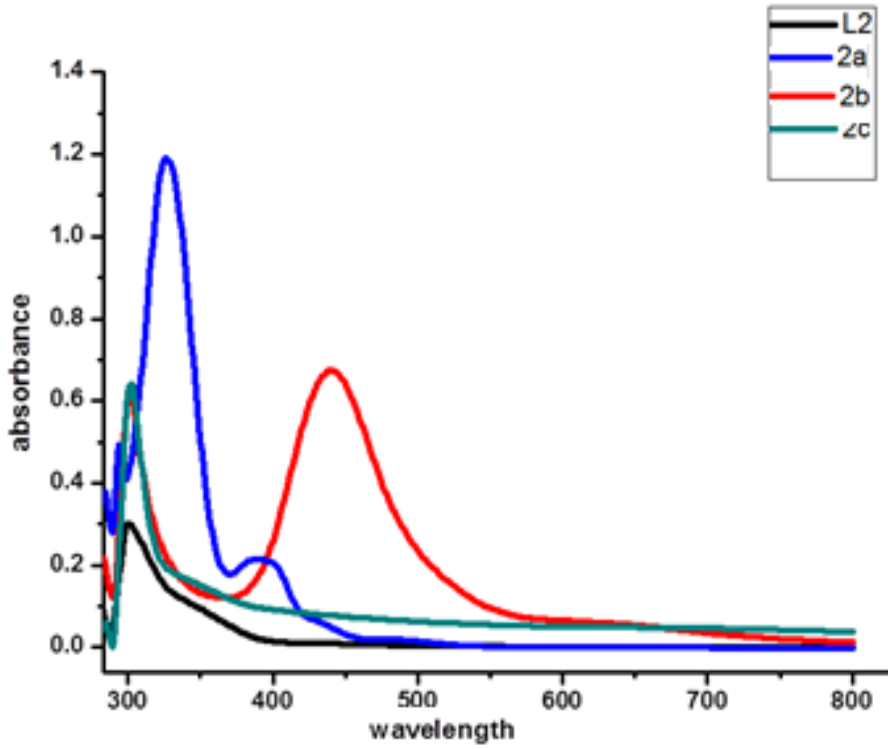

Annexure 39. UV–visible absorption spectra of compounds $\mathbf{L^2}$ and **2a, 2b, 2c** in DMF solution.

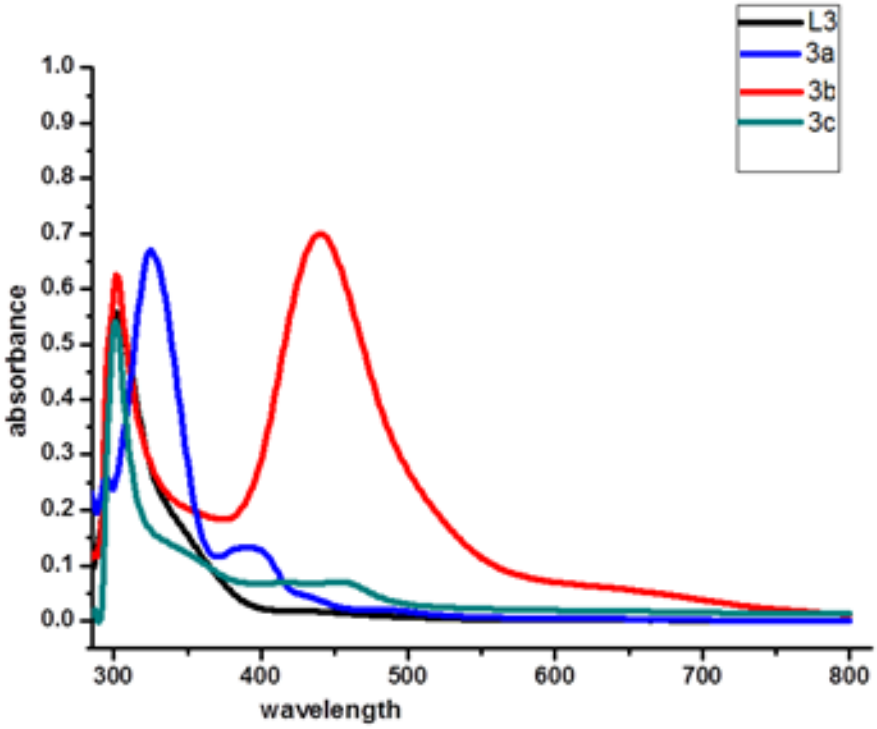

Annexure 40. UV–visible absorption spectra of compounds **L**^{3} and **3a, 3b, 3c** in DMSO solution.

3.6.2 Thermogravimetric study

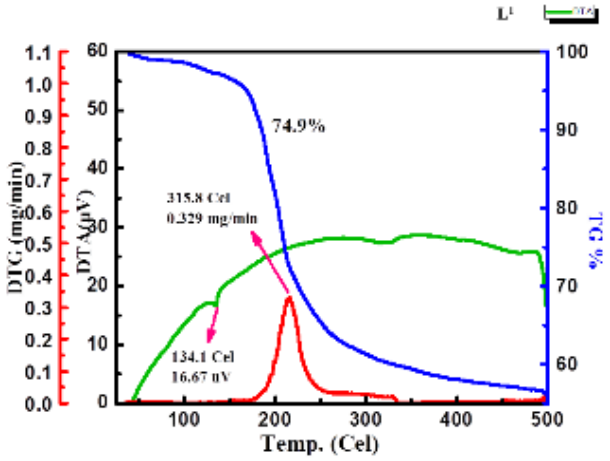

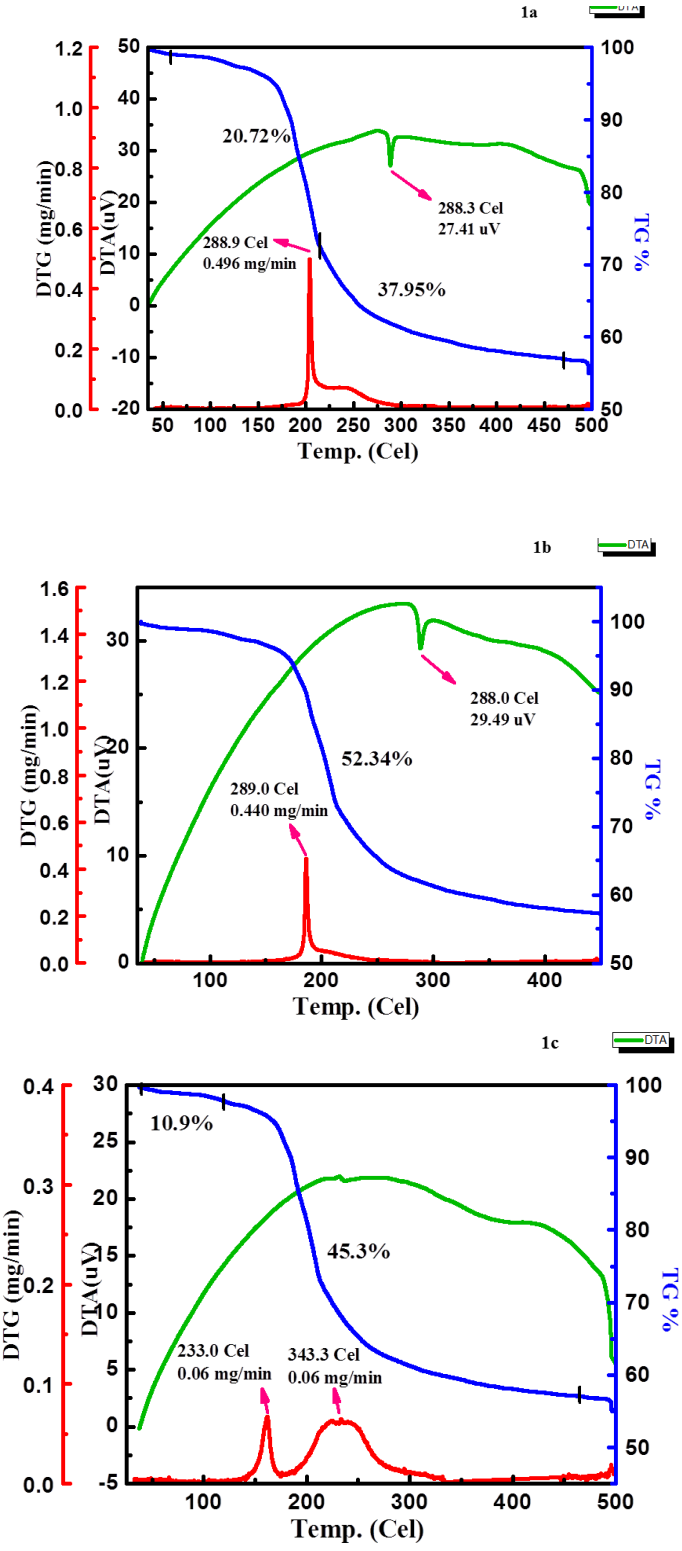

Annexure 41. TGA/DTA plot compounds $\mathbf{L^1}$ and **1a, 1b, 1c**.

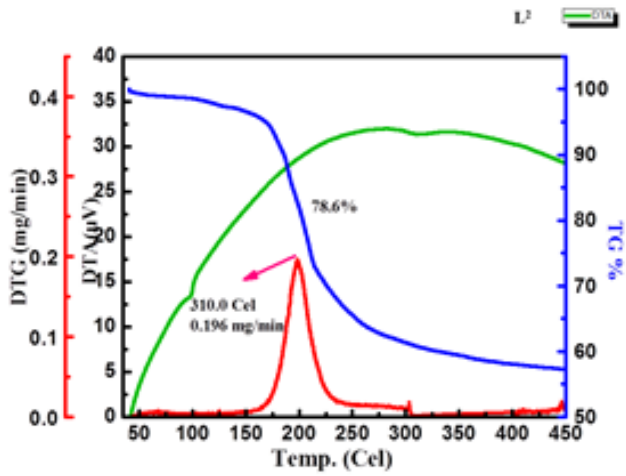
L²
DTG (mg/min)
DTA(uV)
TG %
Temp. (Cel)
78.6%
310.0 Cel
0.196 mg/min

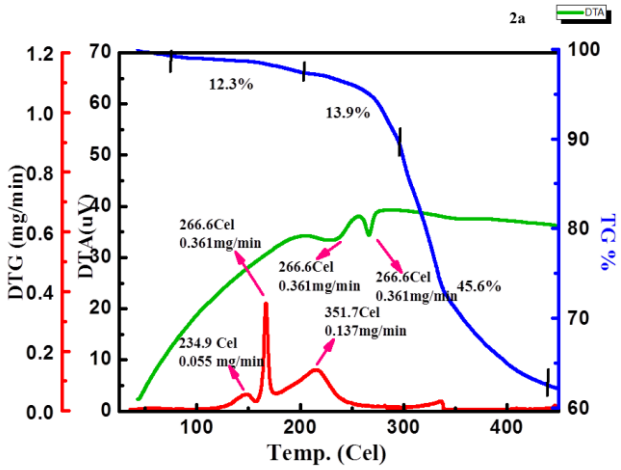
2a
DTA
DTG (mg/min)
DTA(uV)
TG %
Temp. (Cel)
12.3%
13.9%
266.6Cel
0.361mg/min
266.6Cel
0.361mg/min
266.6Cel
0.361mg/min
45.6%
351.7Cel
0.137mg/min
234.9 Cel
0.055 mg/min

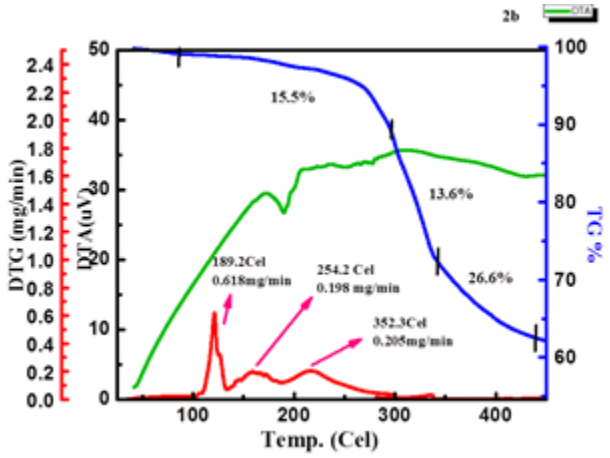
2b
DTA
DTG (mg/min)
DTA(uV)
TG %
Temp. (Cel)
15.5%
13.6%
26.6%
189.2Cel
0.618mg/min
254.2 Cel
0.198 mg/min
352.3Cel
0.205mg/min

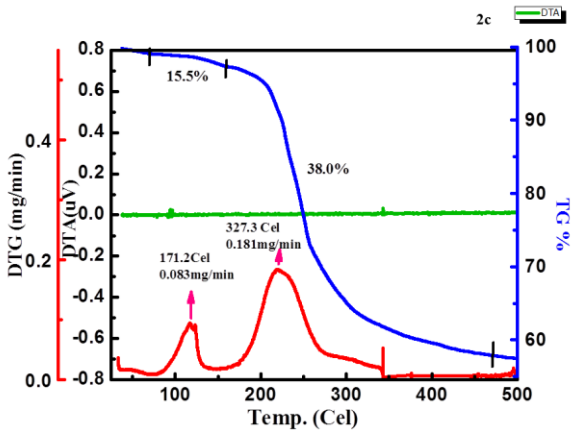

Annexure 42. TGA/DTA plot compounds **L**^{2} and **2a, 2b, 2c**.

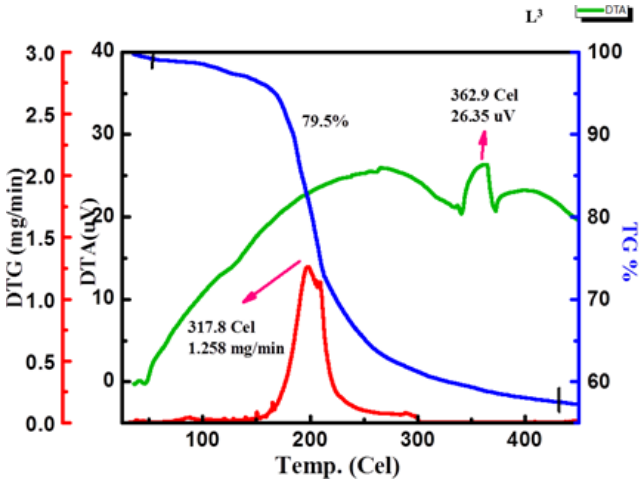

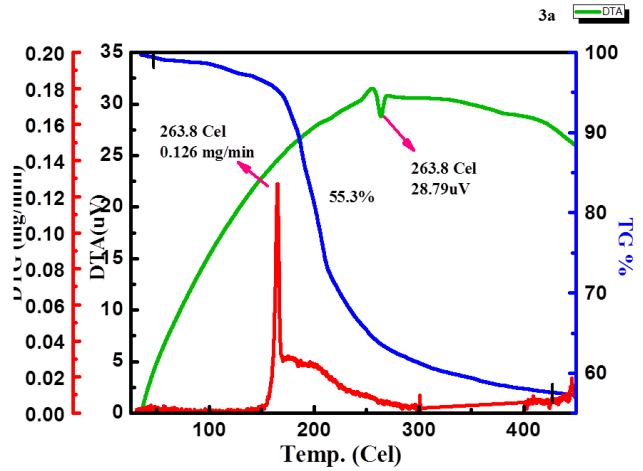

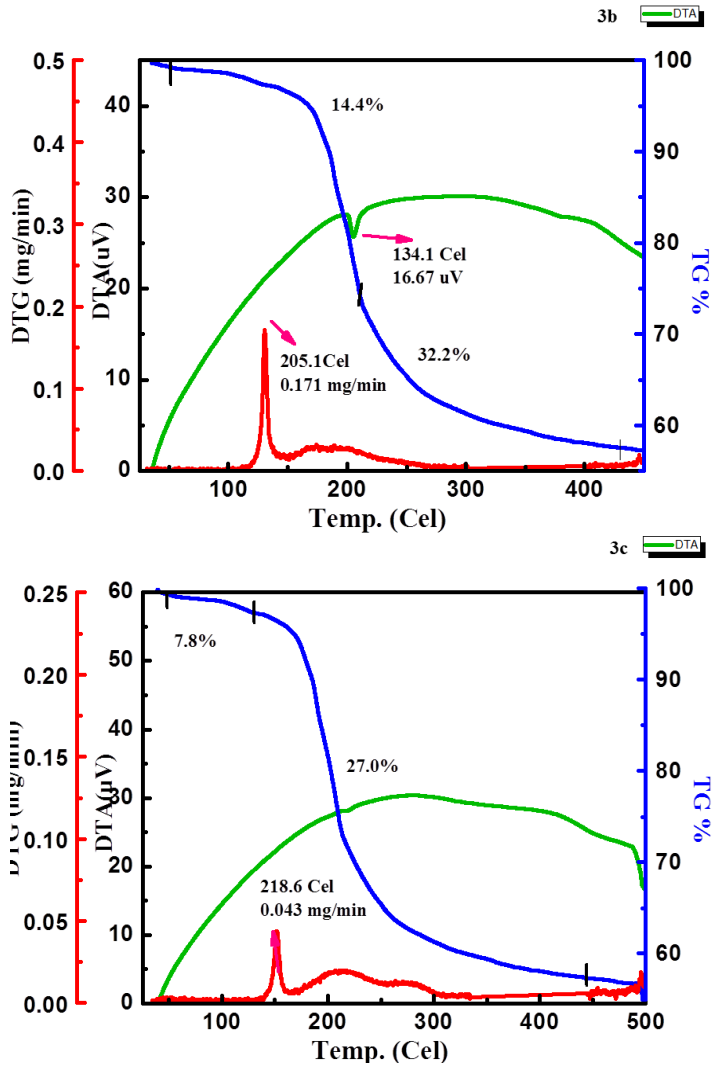

Annexure 43. TGA/DTA plot compounds $\mathbf{L^3}$ and **3a, 3b, 3c**.

The additional supporting Information related to this chapter is provided in the CD as follows:

Chapter 3

1. NMR Spectra: **Figure 1-4**
2. Mass spectra: **Figure 5-8**
3. IR Spectra: **Figure 9-12**
4. Thermogravimetric analysis: **Table 1**
5. Geometry Optimization: **Table 2-5**
6. In vitro cytotoxic study: **Table 6-7** and **figure 13-15**
7. Electrochemical study: **Table 8** and **figure 16.**